A foundation model for atomistic materials chemistry

Ilyes Batatia [†1], Philipp Benner [†2], Yuan Chiang [†3,4], Alin M. Elena [†17], Dávid P. Kovács [†1], Janosh Riebesell [†4,13], Xavier R. Advincula[12,13], Mark Asta[3,4], William J. Baldwin[1], Noam Bernstein[11], Arghya Bhowmik[25], Samuel M. Blau[10], Vlad Cărare[1,13], James P. Darby[1], Sandip De[18], Flaviano Della Pia[12], Volker L. Deringer[16], Rokas Elijošius[1], Zakariya El-Machachi[16], Edvin Fako[18], Andrea C. Ferrari[26], Annalena Genreith-Schriever[12], Janine George[2,6], Rhys E. A. Goodall[15], Clare P. Grey[12], Shuang Han[18], Will Handley[13,19], Hendrik H. Heenen[9], Kersti Hermansson[23], Christian Holm[22], Stephan Hofmann[1], Jad Jaafar[1], Konstantin S. Jakob[9], Hyunwook Jung[9], Venkat Kapil[12, 21], Aaron D. Kaplan[4], Nima Karimitari[20], Namu Kroupa[13,19,1], Jolla Kullgren[23], Matthew C. Kuner[3,4], Domantas Kuryla[12], Guoda Liepuoniute[1,26], Johannes T. Margraf[8], Ioan-Bogdan Magdău[24], Angelos Michaelides[12], J. Harry Moore[1], Aakash A. Naik[2,6], Samuel P. Niblett[12], Sam Walton Norwood[25], Niamh O'Neill[12,13], Christoph Ortner[5], Kristin A. Persson[3,4,7], Karsten Reuter[9], Andrew S. Rosen[3,4], Lars L. Schaaf[1], Christoph Schran[13], Eric Sivonxay[10], Tamás K. Stenczel[1], Viktor Svahn[23], Christopher Sutton[20], Cas van der Oord[1], Eszter Varga-Umbrich[1], Tejs Vegge[25], Martin Vondrák[8,9], Yangshuai Wang[5], William C. Witt[14], Fabian Zills[22], and Gábor Csányi[*1]

[1]Engineering Laboratory, University of Cambridge, Trumpington St and JJ Thomson Ave, Cambridge, UK

[2]Federal Institute of Materials Research and Testing (BAM), Berlin, Germany

[3]Department of Materials Science and Engineering, University of California, Berkeley, CA 94720, USA

[4]Materials Sciences Division, Lawrence Berkeley National Laboratory, Berkeley, CA 94720, USA

[5]Mathematics Department, University of British Columbia, 1984 Mathematics Rd, Vancouver, BC V6T 1Z2, Canada

[6]Institute of Condensed Matter Theory and Solid State Optics, Friedrich Schiller University Jena, Germany

[7]Molecular Foundry, Lawrence Berkeley National Laboratory, Berkeley, California 94720, USA

[8]University of Bayreuth, Bavarian Center for Battery Technology (BayBatt), Bayreuth, Germany

[9]Fritz-Haber-Institute of the Max-Planck-Society, Berlin, Germany

[10]Energy Technologies Area, Lawrence Berkeley National Laboratory, Berkeley, CA 94720, USA

[11]U. S. Naval Research Laboratory, Washington DC 20375, USA

[12]Yusuf Hamied Department of Chemistry, University of Cambridge, Lensfield Road, Cambridge, UK

[13]Cavendish Laboratory, University of Cambridge, J. J. Thomson Ave, Cambridge, UK

[†]These authors contributed equally. All others, except for the corresponding author, are ordered alphabetically.

[*]Corresponding author: gc121@cam.ac.uk

[14]Department of Materials Science and Metallurgy, University of Cambridge, 27 Charles Babbage Road, CB3 0FS, Cambridge, United Kingdom
[15]Chemix, Inc., Sunnyvale, CA 94085, USA
[16]Inorganic Chemistry Laboratory, Department of Chemistry, University of Oxford, Oxford OX1 3QR, UK
[17]Scientific Computing Department, Science and Technology Facilities Council, Daresbury Laboratory, Keckwick Lane, Daresbury WA4 4AD, UK
[18]BASF SE, Carl-Bosch-Straße 38, 67056 Ludwigshafen, Germany
[19]Kavli Institute for Cosmology, University of Cambridge, Madingley Road, Cambridge CB3 0HA, UK
[20]Department of Chemistry and Biochemistry, University of South Carolina, South Carolina 29208, USA
[21]Lennard-Jones Centre, University of Cambridge, Trinity Ln, Cambridge, CB2 1TN, UK
[22]Institute for Computational Physics, University of Stuttgart, 70569 Stuttgart, Germany
[23]Department of Chemistry–Ångström, Uppsala University, Box 538, S-751 21, Uppsala, Sweden
[24]School of Natural and Environmental Science, Newcastle University, Newcastle upon Tyne, NE1 7RU, UK
[25]Department of Energy Conversion and Storage, Technical University of Denmark, Anker Engelunds Vej 301, 2800 Kgs. Lyngby, Denmark
[26]Cambridge Graphene Centre, University of Cambridge, Cambridge, CB3 0FA, UK

January 2, 2024

Machine-learned force fields have transformed the atomistic modelling of materials by enabling simulations of *ab initio* quality on unprecedented time and length scales. However, they are currently limited by: (i) the significant computational and human effort that must go into development and validation of potentials for each particular system of interest; and (ii) a general lack of transferability from one chemical system to the next. Here, using the state-of-the-art MACE architecture we introduce a single general-purpose ML model, trained on a public database of 150k inorganic crystals, that is capable of running stable molecular dynamics on molecules and materials. We demonstrate the power of the MACE-MP-0 model — and its qualitative and at times quantitative accuracy — on a diverse set problems in the physical sciences, including the properties of solids, liquids, gases, and chemical reactions. The model can be applied out of the box and as a starting or "foundation model" for any atomistic system of interest and is thus a step towards democratising the revolution of ML force fields by lowering the barriers to entry.

1 Introduction

Atomic-scale simulation based on density functional theory (DFT) is an enormously successful component of materials modeling (*1–7*). However, the computational cost of such *ab initio* methods, which use electronic structure theory directly, becomes prohibitive for many important cases (e.g., amorphous solids, condensed phase liquids, nanostructured materials, and more). Although fast analytical models in the form of empirical interatomic potentials (or, force fields) have existed for decades, with varying levels of accuracy and applicability (*8*), they generally fail to achieve DFT accuracy, particularly when describing reactive events and phase transitions. As a result, they have been unable to displace DFT for many applications. More

recently, machine learning (ML)-based interatomic potentials, custom-trained for a particular material or system, have improved the achievable accuracy considerably, albeit at a moderate increase in cost relative to empirical force fields (*9–17*). Yet, such custom-trained potentials require significant computational and human effort for the generation of DFT reference data, as well as model training and validation (*18*).

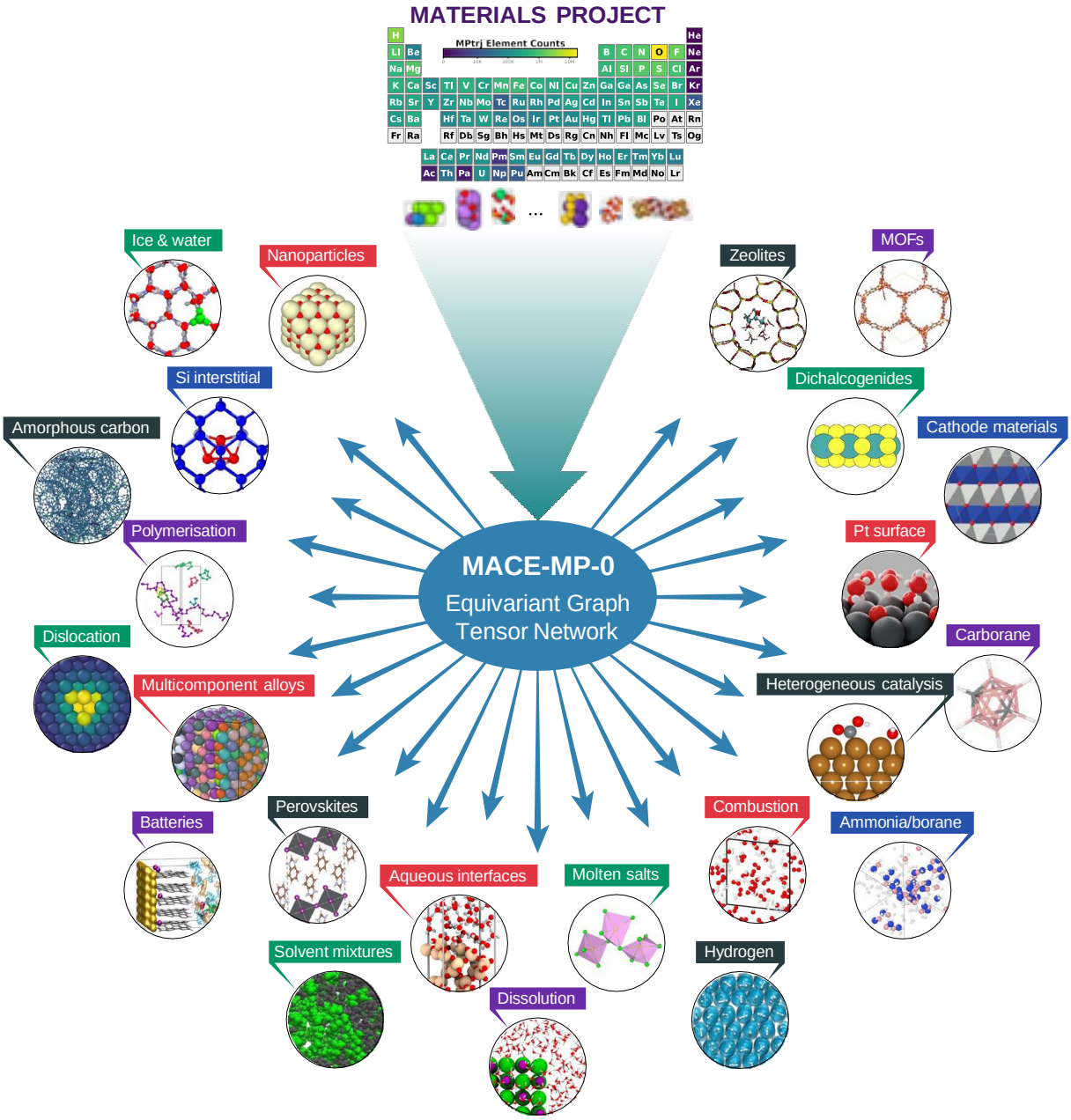

Figure 1: **A foundation model for materials modelling.** Trained only on Materials Project data (*19*) which consists primarily of inorganic crystals and is skewed heavily towards oxides, MACE-MP-0 is capable of molecular dynamics simulation across a wide variety of chemistries in the solid, liquid and gaseous phases.

A pinnacle achievement of ML potentials would be to accurately describe the potential energy surface (PES) across all possible chemical and structural spaces without incurring the high computational cost of *ab initio* electronic structure methods. By enabling robust, accurate molecular dynamics (MD) simulations

for any material, such a potential would enable immediate study of arbitrary systems at a scale currently inaccessible even via the largest available computational resources. (Here, by robustness we mean that the trajectory should not irreversibly end up in unphysical configurations, a frequently observed behaviour for current-generation ML potentials, especially in long multi-nanosecond simulations (*20*).) Particularly desirable applications would include complex chemical reaction processes in both solid and liquid phases, at solid-fluid interfaces, or under pressure.

A key advance towards this goal was made by the MEGNet (*21*) model, which provided property prediction for inorganic crystals, and was trained on minimum energy configurations in the Materials Project (MP) (*19*) that includes most elements of the periodic table (89) and electronic structure calculations using the Perdew-Burke-Enzerhof (PBE) exchange-correlation functional (*22*). More recently, models using equivariant graph neural network architectures with the capacity to compute forces were also trained on MP-based datasets, including M3GNet (*23*) and CHGNet (*24*), which were both trained on snapshots from DFT relaxations of the MP structures, with the CHGNet using the MPtrj dataset introduced at the same time (*24*). The ALIGNN-FF model (*25*) was also trained on a database of inorganic crystals, JARVIS-DFT (*26*), that covers 89 elements and uses the optB88vdW exchange-correlation functional (*27*). The proprietary GNoME (*28*) (NequIP architecture (*16*)) model also starts from MP, but uses a complex active learning workflow to generate and train on a dataset of inorganic crystals nearly two orders of magnitude larger than MPtrj. The above models were created primarily for the purpose of "materials discovery", i.e. predicting thermodynamic stability of hypothetical inorganic crystals. In addition, they were capable of doing molecular dynamics for such crystals, and indeed both CHGNet and GNoME were used to study alkali metal ion diffusion in battery materials. To date, the most general and transferable force field for molecular dynamics is the PFP model (*29*) (TeaNet architecture (*30*)), also proprietary (including its training set that covers 45 elements and is significantly larger than MP and also covers molecules and surfaces). PFP was demonstrated for running simulations on solid state ionic conductors, and a molecular adsorption and a heterogeneous catalysis example. There are also ML force fields specialized for organic molecules (with a much more limited number of elements) such as the ANI (and later AimNET) series of models (*31*–*33*), and also recently for metal alloys (*34*). However, there has yet to be a comprehensive demonstration that a single ML potential can describe solid, liquid, and gaseous systems of materials and molecules across the periodic table and well beyond the distribution of the underlying training set.

Here, we present MACE-MP-0, a new interatomic potential using the MACE architecture (*35*) that is trained just on the MPtrj dataset, and demonstrate its capabilities on an unprecedented range of qualitative and quantitative examples drawn from computational chemistry and materials science, including running stable molecular dynamics simulations in a wide variety of chemistries, predicting phonon spectra, calculating activation energies for point defect and dislocation motion, simulating solvent mixtures, combusting hydrogen gas, modelling a complete rechargeable battery cell, and much more; several of these are illustrated in Fig. 1. We find that this pre-trained *foundation model* shows remarkable out-of-distribution performance.

The MACE architecture was designed to keep only what appear to be essential components of equivariant graph neural networks (*36*): the element embedding with tensor decomposition (*37*) and the higher order equivariant messages constructed through the tensor product operation. Its unique innovations are that (i) it uses high body order equivariant features in each layer (4-body in the present case), and consequently only two layers of message passing are sufficient; (ii) it is only mildly nonlinear, as the only nonlinear activations are in the radial basis and the final readout layer, hence its classification as a graph tensor network. Its computational cost for evaluation is broadly in line with other graph neural networks, presently allowing simulations of around a thousand atoms for nanoseconds per day on a single GPU (depending on atomic density, hardware, floating point precision, size of model, *etc.*, see section A.30 in the Supplementary Information (SI) for details, and when run in parallel using domain decomposition, weak scaling at 0.1 ns/day is perfect up to 32,000 atoms and 64 GPUs on a dense metallic alloy.) The training cost of the model used throughout this paper was about 2,600 GPU hours.

In the following, we highlight three classes of application examples: solid and liquid water, heterogeneous catalysis, and metal–organic frameworks. The SI contains additional examples in 30 separate sections demonstrating the wide-ranging transferability of MACE-MP-0 in predicting properties and dynamic processes of both molecules and materials, as well as benchmarks and graphical exploration of the training data.

2 Applications

2.1 Water and aqueous systems

Water is ubiquitous in nature and technology and has long been a major focus of computational work. Driven by the delicate balance between directional hydrogen bonding and primarily non-directional van der Waals interactions, aqueous systems remain a challenge for simulations (*43*). For example, the study of proton transfer in water, a fundamental process characterized by the continuous breaking and forming of covalent bonds, has long required using *ab initio* molecular dynamics for detailed atomistic insight (*44–46*). We demonstrate in this section how MACE-MP-0 describes various aqueous systems.

We start by examining the structure of liquid water and hexagonal ice (ice Ih). The oxygen–oxygen radial distribution function, depicted in Fig. 2a, shows reasonable agreement with reference simulations. The infrared vibrational spectra of both phases, shown in panel Fig. 2b, align well with experimental observations, albeit with a notable red shift in the stretching vibrations indicating a softer description of the O–H bond as is well-known for PBE-D3 (*43*). In panel Fig. 2d, the relative stabilities of 12 ice polymorphs with respect to ice Ih, used in a recent benchmark (*47*), show excellent agreement with respect to PBE-D3 with a MAE of around 4 meV. Proton defects (OH^- and H_3O^+) in ice Ih and liquid water were simulated, revealing robust descriptions of proton transfer, as shown in Fig. 2c. The proton transfer barrier for hydroxide is higher than for hydronium in liquid water, consistent with experimental diffusion trends.

Next, we evaluate MACE-MP-0 for describing solid–liquid interfaces. First, we focus on NaCl in water in two cases: a NaCl(001) interface in contact with water and a small nanocrystal surrounded by water. Simulations were performed at 400 K to promote dissolution, and compared to simulations with a custom-trained ML potential based on revPBE-D3 from Ref. (*42*). As expected, for the flat surface the model predicts no dissolution events on the timescale of the simulation (0.5 ns). Meanwhile, for the nanocrystal surrounded by water, MACE-MP-0 captures a dissolution mechanism resembling that in Ref. (*42*) as shown in Fig. 2e. The dissolution proceeds via a crumbling mechanism, where an initial steady loss of ions is followed by the rapid disintegration of the crystal. As ions dissolve from the crystal, they are hydrated by water. The dissolution process is stochastic, leading to an intrinsic variation between independent simulations. The final structure of the dissolved ions in water also displays the expected orientation of the water molecules with respect to the ions.

We then model the SiO_2/water interface, Fig. 2f, revealing the expected density modulations in the first few contact layers. As before, the liquid phase is found to be overstructured, a common characteristic of the PBE functional (*43*) used by MP and therefore by MACE-MP-0. SiO_2 is known for its dissociative water adsorption, which we observe in our simulations. Deprotonation of water is evidenced by the shoulder in the water density plot and can also be seen in the inset of a snapshot of this system in Fig. 2f.

Finally, we investigate nanoconfined water in graphene-like nanocapillaries (*48, 49*), which exhibits dramatically different properties from bulk water. MACE-MP-0 proved robust in simulating nanoconfined water. Stable simulations were conducted at 4 GPa and 600 K, conditions under which a superionic phase with high ionic conductivity was previously predicted (*50*) using a custom-trained ML potential. The MACE-MP-0 model accurately captured the dynamical characteristics of this phase, including extensive proton transfer on the ten pico-seconds timescale, as illustrated in the inset of Fig. 2g. Comparing the free energy profile associated with the O– H distance [Fig. 2g] against the PBE-D3 reference, MACE-MP-0 shows an overall good description, albeit underestimating the proton transfer barrier by 1-2 kcal/mol. This tendency towards autoprotolysis is consistent with the soft description of the O– H bond observed in bulk phases.

2.2 Catalysis

The study of heterogeneous (*57–59*) and electrocatalysis (*60–62*) is another major area where DFT excels. It provides atomistic insight into the underlying reaction mechanisms and enables the prediction of the properties of new catalytic materials, (*63*) including reaction barriers and rates, in turn used to predict turnover frequencies (*64*). The latter is essential for the computational discovery of new solid catalysts for overcoming the dependence on rare and toxic elements and improving the efficiency of critical processes for energy conversion. However, the computational cost of DFT is a serious impediment. Empirical interatomic potentials are typically inadequate for catalysis applications as they rarely describe chemical reactions accurately. Machine learning has already had strong impact in computational catalysis (*54,65,66*), *e.g.*, enabling

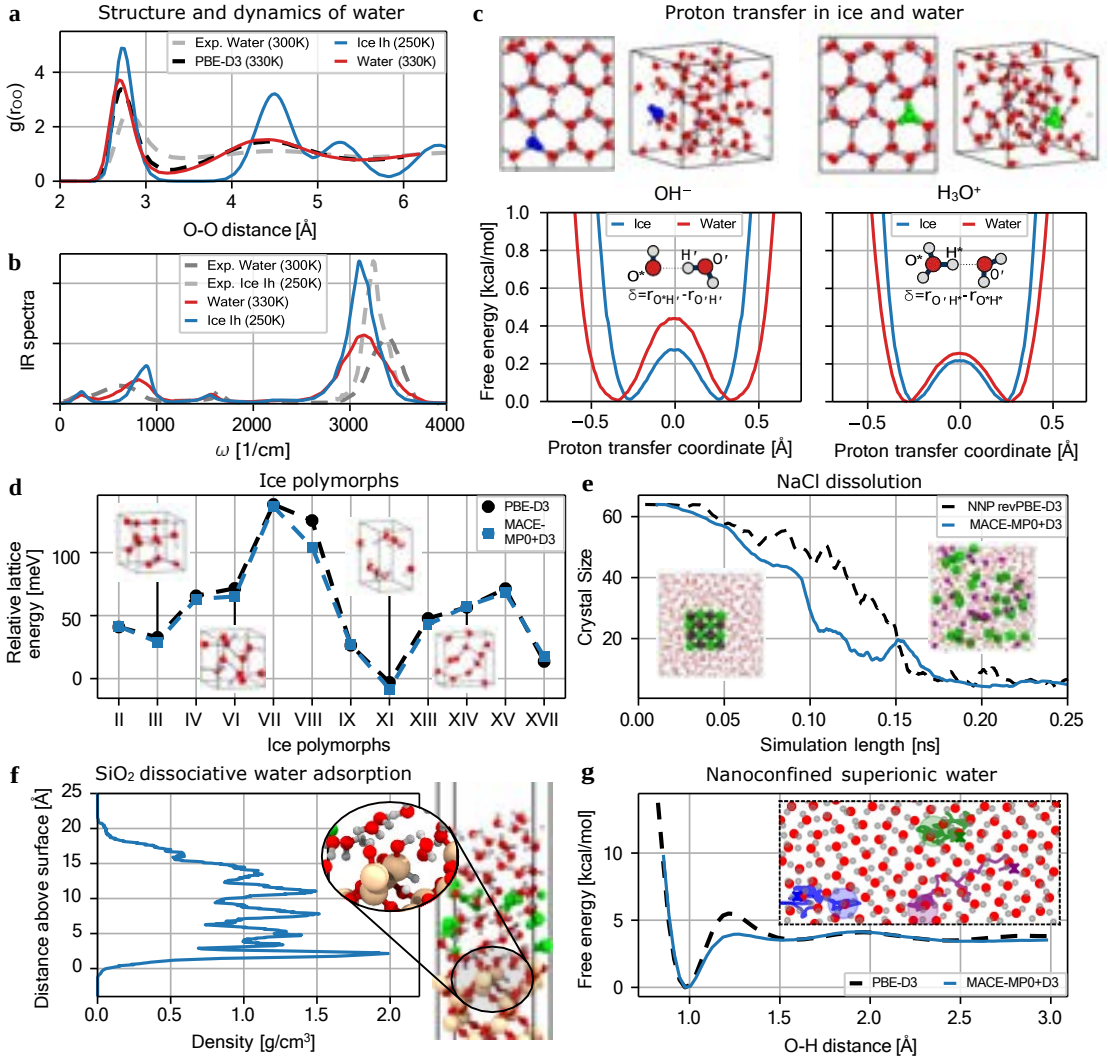

Figure 2: **MACE-MP-0 performance for aqueous systems.** (a) Oxygen–oxygen radial distribution function for bulk water (experimental result from Ref. (*38*)) and ice Ih. (b) Experimental (Ref. (*39*, *40*)) and computed infrared spectra of bulk water and ice Ih. (c) Free energy profiles as a function of the proton transfer barrier for a hydroxide ion and excess proton in ice Ih at 250 K and bulk water at 330 K. Snapshots at the top show the simulation cells. (d) Performance of MACE-MP-0 (blue squares) on the relative lattice energies of the DMC-ICE13 dataset, compared to the reference method, PBE-D3 (*41*) (black circles). (e) Dissolution of a 4 × 4 × 4 unit-cell NaCl nanocrystal in water at 400 K, monitoring the extent of dissolution over the simulation time via the crystal size. Performance of the MACE-MP-0 (blue line) is compared to a neural network potential (*42*) trained explicitly to capture NaCl dissolution (black dashed line). (f) SiO_2/water interface simulation showing density modulations and dissociative water adsorption, with an inset highlighting the deprotonation of water as indicated by a shoulder in the water density plot. H_3O^+ defects in the liquid are highlighted in green. (g) The free energy profile of the O– H distance in the superionic phase of monolayer water in a confining potential. The inset shows a snapshot of the monolayer superionic phase with lines indicating the 50 ps-long trajectory of randomly chosen hydrogen atoms with "×" indicating their initial positions.

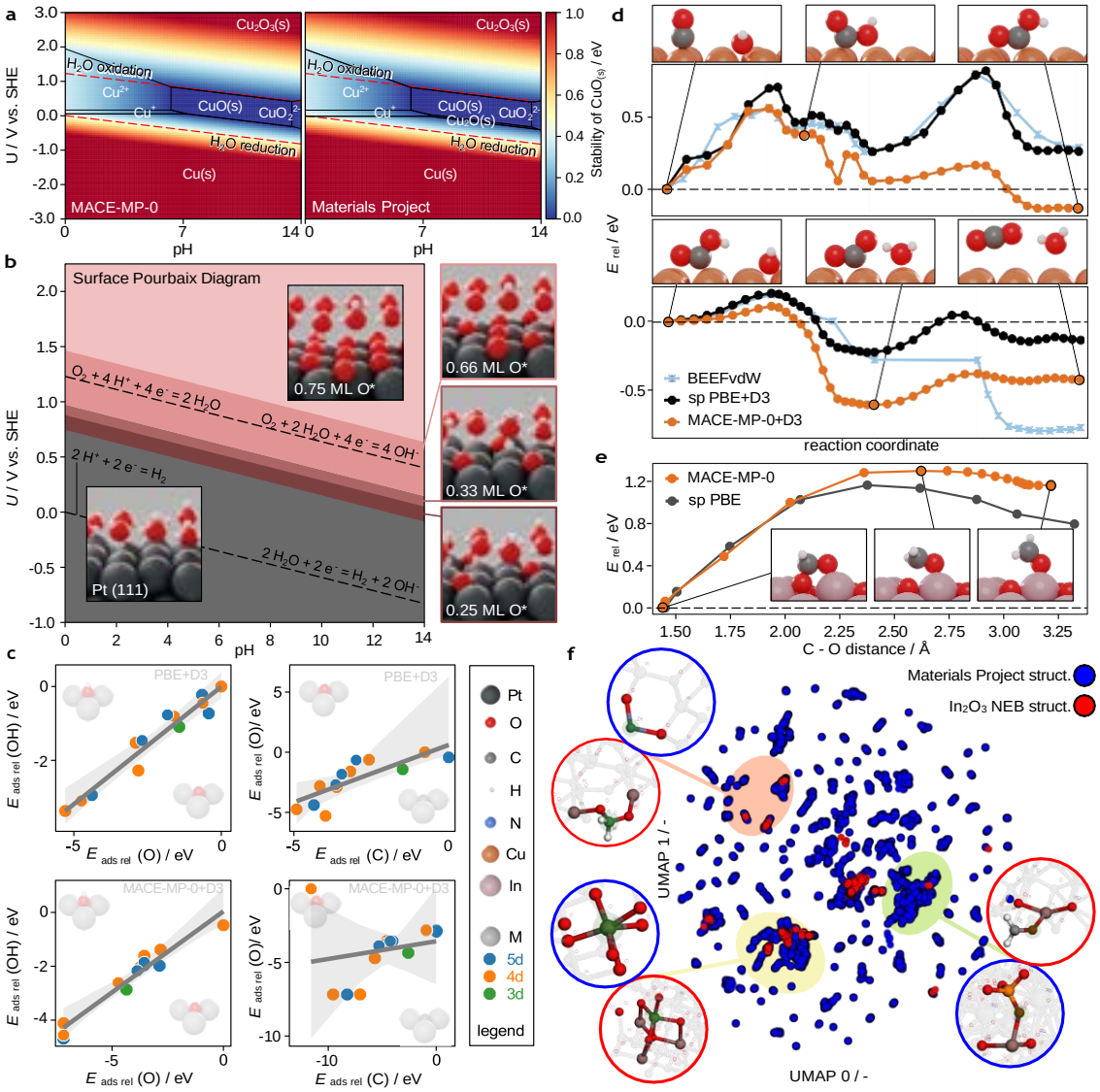

Figure 3: **MACE-MP-0 performance for catalytic applications.** (a) Pourbaix diagrams of CuO bulk systems constructed with MACE-MP-0 (left) and Materials Project reference data (right). (b) MACE-MP-0+D3-calculated Pt(111) surface Pourbaix diagram, in overall good agreement with the literature (*51*). (c) The relative adsorption energy scaling relation between O and OH on transition metal surfaces is captured correctly by MACE-MP-0+D3, as is the lack of linear scaling between C and O (*52*). Metals are colored according to rows in the Periodic Table as 3d, 4d and 5d. (d) Reaction profile of multistep electrochemical CO oxidation on Cu. CO – OH coupling and dehydrogenation reactions are characterised in the upper and lower panel, respectively. Energy profiles from MACE-MP-0+D3 nudged elastic band (NEB) calculations, along with PBE+D3 single-point calculations and independent BEEF-vdW profiles from a previous study (*53*). (e) MACE-MP-0 reaction profile for a key reaction step ($CH_2O_2 \longrightarrow CH_2 + O$) in the CO_2-to-methanol conversion on In_2O_3 (*54*). (f) Comparison of the atomic environments in the training data (blue) and in the In_2O_3 NEB images (red) in the form of a UMAP plot (*55, 56*). Insets show local environments with similar MACE features (inset frames in blue for training data and in red for NEB configurations), exemplifying which bulk training environments influence predictions for the out-of-domain catalytic test case.

fast screening of materials spaces (*67–69*), and free energy calculations beyond the harmonic approximation (*54, 70, 71*). However, developing such accurate potentials from scratch still requires significant human and computational effort. We now test the performance of MACE-MP-0 for different catalysis applications and summarise the results in Fig. 3.

Potential–pH Pourbaix diagrams are central to understanding the aqueous stability of solid materials in an electrochemical environment (*72, 73*), and thus allow predicting the active phase of an electrocatalyst under given conditions. Within the computational hydrogen electrode (CHE) framework (*74*), these diagrams can be computed without an explicit electrostatic model. Figure 3a–b show the MACE-MP-0+D3-calculated Pourbaix diagrams for bulk CuO and a Pt(111) surface. The Pourbaix diagrams are constructed via the formalism described in (*75, 76*), where only the energies of the relevant solids are calculated while corrected experimentally-derived energies are used for the aqueous ions. In both cases, the MACE-MP-0 results show remarkably good agreement with DFT (*51*), predicting the correct sequence of stable phases (with the exception of a very narrow region of Cu_2O stability) and corresponding pH and potential ranges. While this accuracy may be expected for the bulk CuO system that is represented in the training set, the electrosorption at the Pt(111) surface is also well described despite being out of domain.

In Fig. 3c, adsorption energy scaling relations between atomic and hydrogenated adsorbates on transition-metal surfaces are shown for MACE-MP-0+D3 and PBE+D3 (see SI for more examples). Such scaling relations are central to understanding the activity of heterogeneous catalysts (*77, 78*). MACE-MP-0+D3 captures these trends well, and the slopes of the linear fits are in reasonable agreement with DFT (*e.g.* 0.6 for O vs. OH, compared to 0.64 for PBE+D3). Importantly, the lack of correlation between O and C adsorption energies is also captured, indicating that the model is not merely sorting metals according to their general reactivity (*52, 79*). Figure 3d–e show reaction energy profiles for CO oxidation on Cu (*53*) and a key step in CO_2 conversion to methanol on In_2O_3 (*54, 80*), respectively. While these are not quantitatively accurate when compared to DFT, MACE-MP-0+D3 nevertheless captures the location and magnitude of the barriers surprisingly well. Figure 3f illustrates how MACE-MP-0 generalizes to out-of-domain catalysis tasks from bulk training configurations. To this end, the high-dimensional MACE-MP-0 features are projected to 2D using a Uniform Manifold Approximation Projection (UMAP) (*55*), with local atomic environments in the training set shown in blue and those found in the In_2O_3 transition path shown in red. Representative environments with similar MACE-MP-0 features are highlighted, indicating that the internal representation of the atomic environments in the NEB configurations is similar to the representation of under-coordinated environments and metal–organic systems in the training set.

While MACE-MP-0 is not always quantitatively accurate for the most challenging catalysis applications, its stability in MD and exploring reactive pathways is remarkable and provides a starting point for further optimisations. Relevant configurations or phase space regions thus identified may subsequently be validated either by first-principles calculations or serve to initiate active-learning for refining the model. Even at its current foundation level, MACE-MP-0 already allows a statistical sampling far beyond the present DFT-based state of the art which is still largely thermochemistry-centered, whereas MACE-MP-0 will pave the way for true kinetic modeling by explicit evaluations of reaction profiles and the reactive flux along them.

2.3 Metal–organic frameworks

Metal–organic frameworks (MOFs) are a class of nanoporous materials comprised of metal cations or clusters connected by organic linkers arranged in a periodic lattice (*87*). Due to their large surface areas, tunable building blocks, and permanent porosity, MOFs hold substantial promise for various applications, including but not limited to catalysis, energy storage, gas adsorption and separations, and optoelectronic devices (*87*). We tested our pre-trained model directly against version 14 of the Quantum MOF (QMOF) database, which contains DFT-computed properties at several levels of theory for 20,000+ MOFs and structurally related coordination polymers (*81,82*). MACE-MP-0 was not trained on any data from the QMOF database, making this a challenging test of its transferability to largely unseen chemistries.

As shown in Fig. 4a, MACE-MP-0 performs very well in predicting the absolute energies of MOFs, achieving an MAE of 0.033 eV/atom despite the pronounced difference between the inorganic crystals of the MPtrj training set and the MOF structures that make up the QMOF database. This accuracy spans most of the periodic table, as demonstrated in Figure 4b. When the energy prediction is distributed on a per-atom basis, we note a strong elemental dependence of predicted energy error. The higher-than-average errors for

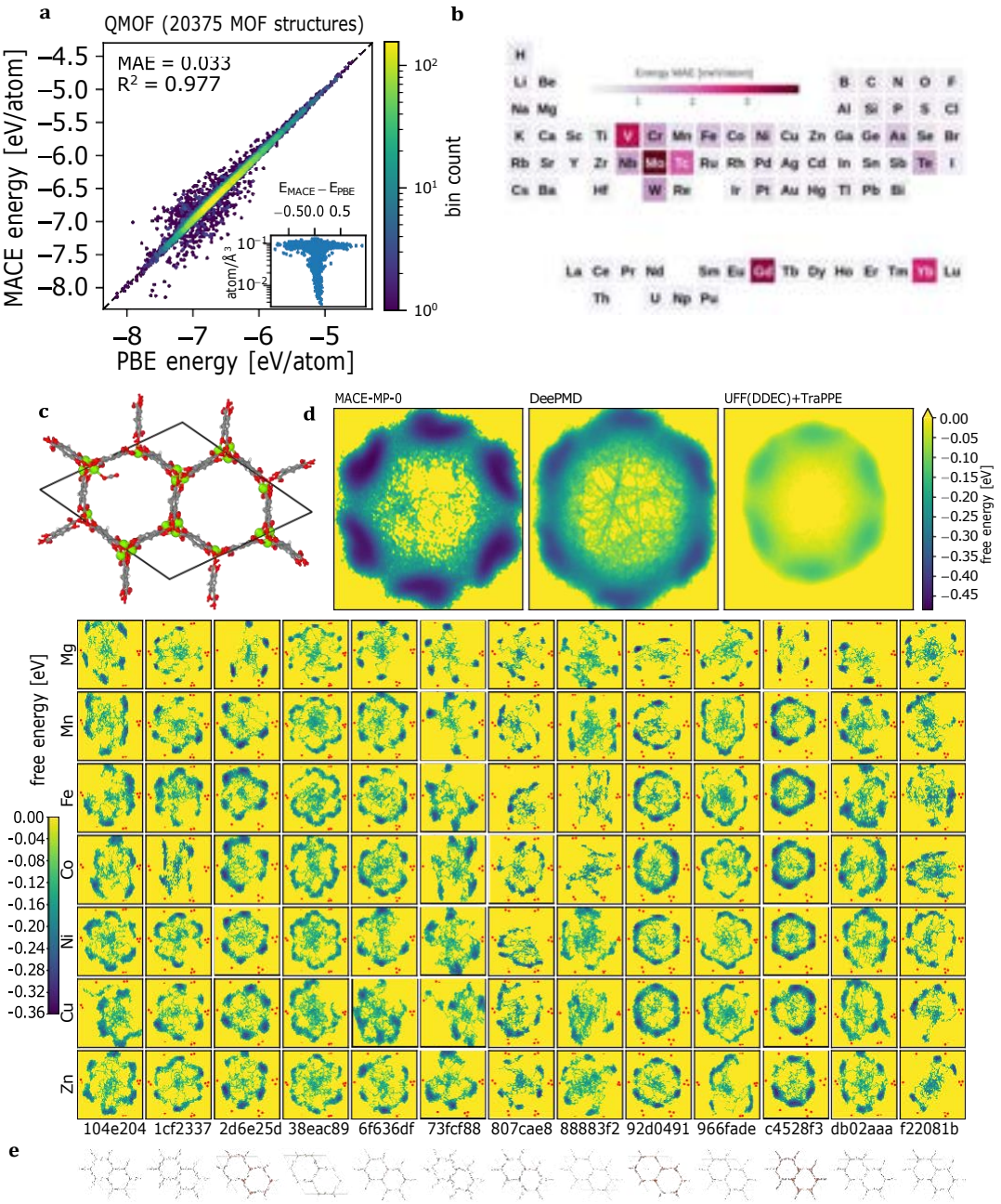

Figure 4: **MACE-MP-0 applied to MOFs.** (a) Comparison between MACE-MP-0 and DFT (PBE) energies on 20,375 relaxed structures taken from the QMOF database (*81*, *82*). (b) Element-wise mean absolute error (MAE) of MACE-MP-0 predicted energies with respect to PBE energies from the QMOF database. The absolute energy error per atom of each structure is distributed over all constituent elements (see SI). (c) Mg-MOF-74 structure with chemisorbed CO_2 optimized with MACE-MP-0. Color key: Mg (orange), O (red), C (brown), H (white). (d) Left: free energy landscape of CO_2 in Mg-MOF-74. Middle: free energy landscape from Ref. (*83*) using a custom-trained DeePMD ML force field. Right: free energy landscape using the UFF classical force field (*84*) with DDEC6 charges (*85*) for the framework and TraPPE for CO_2 (*86*). (e) Free energy maps of 91 hypothetical MOF-74 analogues, with the QMOF ID of the parent Mg-containing frameworks indicated at the bottom of each column and the transition metal to the left of each row.

certain elements (Mo, V, Gd, Yb *etc.*) are due to a difference in the chosen pseudopotentials between the MP and QMOF datasets (see SI 2.3).

To validate the use of MACE-MP-0 for capturing dynamic processes, we investigate CO_2 adsorption in a prototypical MOF known as Mg-MOF-74. The MOF-74 family, including the Mg-containing version, has been extensively studied for the selective adsorption of CO_2 (*88–90*). Of particular note, the coordinatively unsaturated metal sites (*91*) of Mg-MOF-74 enable chemical bonding interactions between the metal and CO_2 adsorbate (*88*) that cannot be captured from classical force fields alone. We directly compare the adsorption dynamics against the results presented in Ref. (*92*), which considered the same system using a custom-trained ML force field generated using DeePMD-Kit (*83*) and PBE-D3 calculations in CP2K (*3*).

MACE-MP-0 accurately and efficiently captures the CO_2 adsorption process in Mg-MOF-74. As shown in Fig. 4c, the CO_2 adsorbate favorably binds to the Mg center in a tilted configuration that is in agreement with both experimental neutron diffraction data (*89, 93*) and the previous custom-trained ML model (*92*). The mean bond distance between the Mg center and CO_2 adsorbate is predicted to be 2.38 Å from MACE-MP-0 (Figure 35a), in close agreement with the experimental value of 2.27 Å (*89*) and the value of 2.23 Å from the custom ML model in Ref. (*92*). The mean Mg – O– C bond angle is predicted to be 133.7° from MACE-MP-0 (Fig. 35a), substantially closer to the experimentally determined bond angle of 131° (*89*) than the 118.6° value from the ML model in Ref. (*92*). The projected density map for the CO_2 adsorption site (Fig. 4b) is, again, in excellent agreement with prior work (*92, 93*) and shows how the adsorbed CO_2 molecules are mobile but largely confined to the vicinity of the Mg binding site due to chemisorption.

To showcase an example of how one might use MACE-MP-0 in a high-throughput setting, we considered 91 hypothetical MOF-74 analogues derived from those in Ref. (*94*) based on 13 (out of 58) different frameworks and seven different metal cations (M) that have been used to synthesize M-MOF-74 (*89*). Figure 4e shows the resulting free energy maps, comprising over 160 ns of simulation altogether, displaying diverse and dynamic behaviour of the CO_2 adsorbate across the range of hypothetical MOF-74 analogues.

Given the nature of our foundation model, we anticipate many additional application areas where MACE-MP-0 (or one of its future variants) could be of value in the MOF field. Based on the CO_2 adsorption example, we envision applications in capturing dynamic processes, particularly those that cannot be accurately modeled using classical force fields and are prohibitively expensive to carry out with *ab initio* MD given the large unit-cell size required to describe most MOFs. Foundation models are promising for modeling competitive multi-component physisorption and chemisorption processes, especially across many families of compositionally different MOFs and combinations of gas mixtures, for which training a system-specific, on-the-fly active learning model would be expensive or even prohibitive. In addition to the compositional diversity relevant to high-throughput screening, not all MOFs can be described via a static picture and based on an ideal crystalline structure: in fact, there has been recent interest in liquid and amorphous MOFs (*95, 96*), and the dynamic behavior of crystalline frameworks (*97*) — such as in the so-called "flexible" and "breathing" MOFs — has been leveraged for highly selective separation processes (*98*). This dynamic behavior cannot be completely captured from static DFT calculations alone, and accurate and easily accessible interatomic potentials are expected to accelerate the modeling of spatio-temporal processes in future studies (*99*).

2.4 Further applications and Supplementary Information

In the Supplementary Information in 30 subsections, we provide further application examples. We also give the results of a comprehensive set of benchmarks, including the performance on calculating phonon dispersions, bulk and shear moduli of crystals, atomisation energies and lattice constants of elemental solids, the cohesive energies of the S66 set (*100*) of molecular dimers and the X23 set (*101*) of molecular crystals, the CRBH20 set (*102*) of reaction barrier heights, and the homonuclear diatomic binding curves. The full set of heteronuclear diatomic curves is provided in the Supplementary Materials.

We also give more details on the training protocol, and a graphical exploration of the data, including histograms of energies, forces, stresses, magnetic moments, and element and composition counts.

3 Current limitations and future outlook

The DFT-quality simulation and stable MD propagation for a wide range of materials across the periodic table that we have shown here are landmark achievements for a single machine-learned interatomic potential. Yet there are a number of limitations of the current version of the MACE-MP-0 model. The exchange-correlation functional used in the MPtrj dataset is PBE (*22*), which must be augmented with Hubbard U terms to improve electronic correlations for particular element combinations (introducing inconsistencies in the PES that must be compensated (*6*)), and dispersion corrections, such as D3 (*41*). Recent developments in DFT are beginning to supersede it by achieving improved accuracy at comparable computational cost (*103, 104*), and methods beyond DFT such as hybrid functionals (*105*) and the random phase approximation (*106*) improve upon this even further but at much larger computational cost. Refitting the model to a more modern functional is expected to increase its predictive power, and will reduce the need for system-dependent corrections such as the use of Hubbard U terms and dispersion.

The MACE model that we used to fit the data does not contain explicit long range interactions (beyond the 12 Å receptive field afforded by two steps of message passing), nor does it take into account magnetic or spin degrees of freedom. Despite the success in describing many different chemistries demonstrated herein, there will be observables, particularly in the context of dilute solutions and at interfaces, that cannot be calculated with a short-range model. There are several approaches to incorporating explicit electrostatic interactions into ML models in the literature (*107–110*), as well as spin degrees of freedom (*24, 111, 112*). A subsequent version of our model will undoubtedly benefit from such an extension.

Considering the results for the diverse systems shown in the SI, there are two broad areas where the model clearly needs improvement: (i) describing intermolecular interactions, (ii) high pressure simulations. While the overarching goal of MD stability is achieved for ambient conditions, for many systems there is room for improvement in a quantitative sense. In some cases, e.g. low pressure simulations of ethanol (section appendix A.16), these small quantitative deviations lead to qualitative errors by shifting an important phase transition's temperature or pressure, thereby changing the equilibrium phase at ambient conditions. In other cases, namely atoms that approach each other at very close distances in random structure search (section appendix A.14) or high pressure hydrogen (section appendix A.21), the energy errors are large, and the simulations become trapped in anomalously low energy, unphysical geometries. These errors are not specific to certain systems, and both can be addressed straightforwardly by extending the existing training data to lower and higher pressures (*113*) for the former, and using repulsive pair potentials (*114*) for the latter. In most cases, it is not yet wise to solely rely on ML potentials for all chemical or physical predictions without further validation (*115*), and the same is true for MACE-MP-0.

Several possible factors may be limiting the model's accuracy: the size of the model in terms of number of free parameters and the limits this places on its expressivity, the total amount and type of configurations in the training set, or inconsistencies in the quantum-mechanically computed data labels. Exploration of possible improvements to the model and its training data is ongoing to determine which of these are responsible for current limitations. The results will determine in what ways the model and its improved versions will be used in the future.

The most pessimistic, but we think unlikely, possibility is that using MACE-MP-0 as a foundation model that must be fine-tuned to give quantitative accuracy for specific systems will require very large amounts of data and/or training time, and that the pre-trained model will not provide a significant shortcut compared to training models from scratch. In this case, the ability of MACE-MP-0 to produce *reasonable* trajectories will still make it useful as an efficient source of configurations for system-specific fitting databases, perhaps augmented by further active learning.

A more likely scenario is that the current model will at least be able to serve as a starting point that can be efficiently fine-tuned for any particular system. It remains to be seen how much additional data would be needed for such refinement, but based on previous experience we are optimistic; pre-training with cheaply generated data and subsequent fine-tuning has been shown to improve accuracy and stability of ML potentials (*116*), and transfer-learning approaches can enable such models to fit higher quality reference data (*32*). This type of refinement will definitely be required for systems where the level of theory that was used to calculate the currently used training dataset are considered to be inadequate. There is good evidence that reaching higher levels of electronic structure theory from a DFT baseline and beyond requires significantly less data than fitting to DFT itself (*32, 117, 118*)

Finally, we may find that adding only a moderate number of additional configurations computed with essentially the same methodology will be sufficient to achieve quantitative agreement with the target level of theory across the full range of chemistry and structure. If this turns out to be true, future versions of MACE-MP-0 may truly provide a universal model for carrying out material simulations.

4 Methods

4.1 Model

MACE All models trained in the paper use the MACE (*35*) architecture implemented in PyTorch (*119*) and employing the *e3nn* library (*120*). The MACE training and evaluation codes are distributed via GitHub under the MIT license. MACE is an equivariant message-passing graph tensor network where each layer encodes many-body information of atomic geometry. At each layer, many-body messages are formed using a linear combination of a tensor product basis (*36, 37*). This is constructed by taking tensor products of a sum of two-body permutation-invariant polynomials, expanded in a spherical basis. The final output is the energy contribution of each atom to the total potential energy. For a more detailed description of the architecture, see Refs. (*35*) and (*121*).

Hyper-parameters All models referred to in this work use two MACE layers, a spherical expansion of up to $l_{\max} = 3$, and 4-body messages in each layer (correlation order 3). All models use a 128-channel dimension for tensor decomposition. We use a radial cutoff of 6 Å and expand the interatomic distances into 10 Bessel functions multiplied by a smooth polynomial cutoff function to construct radial features, in turn fed into a fully-connected feed-forward neural network with three hidden layers of 64 hidden units and SiLU non-linearities. We fit three different size models, which only differ by the maximal message equivariance, $L = 0, 1, 2$ for the small, medium and large models, respectively, and provide different compromises between computational cost and fitting accuracy. All application examples in this paper are run with the medium $L = 1$ model as it offers a good cost-accuracy trade-off.

Normalization To ensure internal normalization of the weights, we divide the atomic basis in each layer by the average number of neighbors in the training dataset, as proposed in (*36*). This number is fixed at ≈ 62. The node energy ϵ_a of atom a is shifted by the mean of the atomic energies. Therefore, the prediction of the energy for the whole structure is constructed as

$$\hat{E} = \sum_{a=1}^{N} \left(\sigma \left(\sum_{k=1}^{K} \epsilon_a^{(k)} \right) + \mu_{Z_a} \right)$$

where K denotes the total number of message passing layers and $\epsilon_a^{(k)}$ is the energy of atom a at layer k. μ and σ are the mean atomic energies and the mean square of the atomic forces computed on the training set. The predicted forces and stresses are computed as derivatives of the total energy with respect to the atomic positions and the strain tensor, respectively.

Training loss The models were trained using a weighted sum of Huber losses of energy, forces, and stress:

$$\begin{aligned} L = & \frac{\lambda_E}{N_b} \sum_{b=1}^{N_b} L_{\text{Huber}} \left(\frac{\hat{E}_b}{N_a}, \frac{E_b}{N_a}, \delta_E \right) \\ & + \frac{\lambda_F}{3 \sum_{b=1}^{N_b} N_a} \sum_{b=1}^{N_b} \sum_{a=1}^{N_a} \sum_{i=1}^{3} L'_{\text{Huber}} \left(\frac{\partial \hat{E}_b}{\partial r_{b,a,i}}, F_{b,a,i}, \delta_F \right) \\ & + \frac{\lambda_\sigma}{9 N_b} \sum_{b=1}^{N_b} \sum_{i=1}^{3} \sum_{j=1}^{3} L_{\text{Huber}} \left(\frac{1}{V_b} \frac{\partial \hat{E}_b}{\partial \varepsilon_{b,ij}}, \sigma_{b,ij}, \delta_\sigma \right), \end{aligned} \tag{1}$$

where λ_E, λ_F , λ_σ are predetermined weights of energy (E), forces (F), and stress (σ) losses, the symbols under a hat correspond to predicted values, and N_b and N_a are the batch size and the number of atoms in each structure. In the last term involving the stress, ε_b and σ_b correspond to the strain and stress tensors, respectively. We used $(\lambda_E, \lambda_F, \lambda_\sigma) = (1, 10, 100)$ and Huber deltas of $\delta_E = 0.01, \delta_F = 0.01, \delta_\sigma = 0.01$. We use a conditional Huber loss L'_{Huber} for forces, where the Huber delta δ_F is adaptive to the force magnitude on each atom. The Huber delta δ_F decreases step-wise by a factor from 1.0 to 0.1 as the atomic force increases from 0 to 300 eV/Å. For more details, see the section C.1 in th SI.

Optimization The models are trained with the AMSGrad (*122*) variant of Adam (*123*) with default parameters $\beta_1 = 0.9$, $\beta_2 = 0.999$, and $\epsilon = 10^{-8}$. We use a learning rate of 0.001 and a exponential moving average (EMA) learning scheduler with decaying factor of 0.995. We employ a gradient clipping of 100. Models are trained for 200 epochs on 40–80 NVIDIA A100 GPUs across 10–20 nodes. Training the medium-sized model took approx. 2,600 GPU hours.

Training data The MACE-MP-0 model was trained on the MPtrj dataset which was compiled originally for CHGNet (*24*). This dataset consists of a large number of static calculations and structural optimization trajectories from the Materials Project (MP) (*19*). These include approx. 1.5M configurations (roughly ten times the approx. 150k unique MP structures), mainly small periodic unit cells (90% under 70 atoms) describing inorganic crystals with some molecular components. The DFT calculations use the PBE exchange-correlation functional with Hubbard U terms applied to some transition metal oxide systems, but no additional dispersion correction (*124*).

Since the potential we fit calculates the energy based only on structural information, ideally we would like to use consistent electronic calculation parameters and the lowest energy electronic state for each configuration. One significant source of inconsistency is the application of Hubbard U, which is used in MP calculations only when O or F are present together with any of 8 transition metals (Co, Cr, Fe, Mn, Mo, Ni, V, W) (*125*). The application of U leads to a shift in energy correlated with the value of U, *i.e.* a few eV, not explicitly accounted for in our fit. Thus, energies from calculations using those 8 elements with and without O or F are inconsistent (in the sense that the energy along a continuous deformation path that removes the O or F atoms from around these metals would be discontinuous). The pre-trained CHGNet fit to MPtrj used energies corrected to account for the presence or absence of U (*126*). In our fit, this shift only occurs between structures with different compositions and for any given composition the energies should be consistent. As a result, we expect configurations that include local regions of these metals with very different O or F content, *e.g.* an interface between a metal and an oxide, may be poorly described.

In addition, the current fitting database includes a variety of magnetic orders generated as part of a systematic search for the magnetic ground state (*127*), chosen from the full database only based on calculation type ("GGA Static" and "GGA Structure Optimization") and energy-difference criteria (*24*). To quantify the effect of this additional and unaccounted-for degree of freedom, we classify the magnetic order associated with each calculation task into one of four categories: 1) no atomic magnetic moment listed, 2) moment converged to zero on all atoms, 3) converged to ferromagnetic order, and 4) converged to another magnetic order. Of the approx. 150k MP-IDs present, about 48k have more than one magnetic order present in the fitting database. In the vast majority of cases, this includes a calculation where the moments are *unknown* (*i.e.* not recorded) and a single other magnetic order, and we can hope that they are actually consistent. However, for 5186 MP-IDs we find multiple non-trivial magnetic orders. To quantify the effect on the fitting quantities, we calculate the minimum energies of each magnetic order for each material, and analyze the range of minima values seen for each material (distribution is plotted in SI Fig. 50). While the vast majority of materials have negligible variation, there are hundreds with variation >100 meV/atom (*i.e.* an order of magnitude larger than the energy error on the validation set), and a few that vary by <0.5 eV/atom.

Long-range dispersion corrections Dispersion interactions, sometimes called van der Waals interactions, are crucial for describing the weak, long-range interactions between electrons. Common approximations in DFT, such as PBE (*22*), cannot capture such long-ranged interactions, motivating the use of additive non-local corrections, such as DFT-D3 (*41*) or rVV10 (*128*). Inclusion of a dispersion correction to DFT is necessary to describe the dynamics of liquid water (*129*), the geometries and binding energies of layered solids (*130*), and stability of metal–organic frameworks (*131*), among many other examples.

Additive dispersion corrections typically employ a physical model for dispersion interactions with empirical parameters optimized to cut off the correction at interatomic distances where approximate DFT is reliable. DFT-D3 is an interatomic potential which uses tabulated values of atomic polarizabilities to describe two-body and, optionally, three-body Axilrod–Teller (*132*) dispersion interactions. As MACE-MP-0 is trained to PBE energies, forces, and stresses, it inherits PBE's lack of long-range dispersion interactions. An optional, additive DFT-D3 dispersion correction can be applied to MACE-MP-0. The PyTorch implementation of DFT-D3 used in this work is described in Ref. (*29*). The same parameters used in PBE-D3(BJ), i.e., DFT-D3 with a Becke-Johnson damping function (*133*), are used in the D3 correction to MACE-MP-0.

Author contributions

Model training: YC, PB, IB; **Data/Model analysis:** PB, YC, JR, NB, RE, MCK, ES; **MACE code:** IB, YC, SWN, DPK, PB, WCW; **Application examples:** WJB ($CsPbI_3$, appendix A.5); LLS (catalysis: In_2O_3, section 2.2 and appendix A.23.4); IB (a-C quenches, appendix A.3.1); ZEM (a-C graphitisation, appendix A.3.2); NK (Si interstitials, appendix A.1); EVU, XRA, NON (aqueous interfaces, section 2.1 and appendix A.18); YC (molten salts, appendix A.19); CSc, VK, FDP, XRA (water and ice, section 2.1 and appendix A.15); SPN and AGS ($LiNiO_2$, appendix A.11); SWN (lithiated graphite, appendix A.10); AME (zeolites appendix A.9); JJ (transition metal dichalcogenides, appendix A.25); JHM (ethanol/water, appendix A.16, trialanine, appendix A.29); GL (a-Si appendix A.2); DK (carborane, appendix A.24, ammonia-borane, appendix A.22); VC (S polymerisation, appendix A.8); JR, JG and AAN (phonons, appendix B.1); JR, REAG (materials discovery: formation energy, appendix A.28.1); KSJ (materials discovery: stoichiometric substitutions, appendix A.28.2); ADK (materials discovery: highly-coordinated structures, appendix A.28.3); ASR, YC and AME (MOFs, section 2.3 and appendix A.27); MV (solvent mixtures, appendix A.17); DPK, ES, SMB (hydrogen combustion, appendix A.7); NKa, CSu (HOIPs, appendix A.6); CO, YW (dislocation, appendix A.12); WCW (HEA, appendix A.30); EF, SD (catalysis: linear scaling relationships, section 2.2 and appendix A.23.2); HJ, HHH (catalysis: CO oxidation on Cu, section 2.2 and appendix A.23.3); SH, SD (catalysis: Pourbaix diagrams, section 2.2 and appendix A.23.1); MCK (benchmarks: bulk and shear moduli, appendix B.2); FDP (benchmarks: cohesive energies and lattice constants of solids, appendix B.3, atomization energies appendix B.4, and reaction barrier heights, appendix B.5); TKS (Al_2O_3, appendix A.13, diatomics, appendix B.6); JPD (Arsenic random structure search, appendix A.14); IBM (high-pressure hydrogen, appendix A.21, and electrode-electrolyte interface / battery system, appendix A.26); JK, VS and KH (CeO_2, appendix A.4); FZ (ionic liquids, appendix A.20) **Supervision:** AB, ACF, AM, ASR, CH, CO, CPG, CSu, GC, HHH, JG, JK, JTM, KAP, KH, KR, MA, SD, SMB, TV, VLD, WH, WJB; **Drafted manuscript:** IB, NB, YC, GC, SD, HHH, MCK, JR, ASR, CSc, JTM; **Edited manuscript:** IB, NB, YC, GC, VLD, JG, REAG, JR, MCK, KAP, ASR, LLS, JTM, AM, CO, AME, WCW.

Acknowledgments

Model training made use of resources of the National Energy Research Scientific Computing Center, a DOE Office of Science User Facility supported by the Office of Science of the U.S. Department of Energy under contract no. DE-AC02-05CH11231 using awards BES-ERCAP0023528 and BES-ERCAP0022838. Part of this work was performed using the Cambridge Service for Data-Driven Discovery (CSD3), part of which is operated by the University of Cambridge Research Computing on behalf of the STFC DiRAC HPC Facility (www.dirac.ac.uk). The DiRAC component of CSD3 was funded by BEIS capital funding via STFC capital grants ST/P002307/1 and ST/R002452/1 and STFC operations grant ST/R00689X/1. DiRAC is part of the National e-Infrastructure. The work of YC, JR, ADK, MCK, MA and KAP was supported by the US Department of Energy, Office of Science, Office of Basic Energy Sciences, Materials Sciences and Engineering Division, under contract no. DE-AC02-05-CH11231 (Materials Project program KC23MP). We could not have done this work without the DFT relaxation trajectories freely provided by the Materials Project and carefully curated into the MPtrj training set by Bowen Deng (*24*). JR acknowledges support from the German Academic Scholarship Foundation (Studienstiftung). YC acknowledges financial support from UC Berkeley and Taiwan-UC Berkeley Fellowship from the Ministry of Education in Taiwan. MCK acknowledges support by the National Science Foundation Graduate Research Fellowship Program under Grant No. DGE-2146752. Any opinions, findings, and conclusions or recommendations expressed in this work are those of the author(s) and do not necessarily reflect the views of the National Science Foundation. NB was supported by fundamental-research base-program funding from the U.S. Naval Research Laboratory. ASR acknowledges support via a Miller Research Fellowship from the Miller Institute for Basic Research in Science, University of California, Berkeley. LLS acknowledges support from the EPSRC Syntech CDT with grant reference EP/S024220/1. AM and XRA acknowledge support from the European Union under the "n-AQUA" European Research Council project (Grant no. 101071937). SWN, AB, TV acknowledge support from the European Union's Horizon 2020 research and innovation program under the Marie Skłodowska-Curie Actions (Grant Agreement 945357) as part of the DESTINY PhD program. GC, CPG, TV, AB and

SWN acknowledge support from the European Union's Horizon 2020 research and innovation program under Grant Agreement 957189 (BIG-MAP). VK acknowledges support from the Ernest Oppenheimer Early Career Fellowship and the Sydney Harvey Junior Research Fellowship, Churchill College, University of Cambridge. V.K. acknowledges computational support from the Swiss National Supercomputing Centre under project s1209. ZEM acknowledges support from the EPSRC Centre for Doctoral Training in Theory and Modeling in Chemical Sciences (TMCS), under grant EP/L015722/1. VLD acknowledges support from the John Fell OUP Research Fund. CH and FZ acknowledge support by the Deutsche Forschungsgemeinschaft (DFG, German Research Foundation) in the framework of the priority program SPP 2363, "Utilization and Development of Machine Learning for Molecular Applications - Molecular Machine Learning" Project No. 497249646 as well as further funding though the DFG under Germany's Excellence Strategy - EXC 2075 - 390740016 and the Stuttgart Center for Simulation Science (SimTech). AME's work used the DiRAC Extreme Scaling service (Tursa) at the University of Edinburgh, which is part of the STFC DiRAC HPC Facility (www.dirac.ac.uk) and scarf cluster (www.scarf.rl.ac.uk/) maintained by Scientific Computing Department STFC. AME's access to DiRAC resources was granted through a Director's Discretionary Time allocation in 2023/24, under the auspices of the UKRI-funded DiRAC Federation Project. AME's work was also supported by Ada Lovelace centre at STFC (https://adalovelacecentre.ac.uk/), Physical Sciences Databases Infrastructure (https://psdi.ac.uk) and EPSRC under grants EP/W026775/1 and EP/V028537/1. IB, RE and NK were supported by the Harding Distinguished Postgraduate Scholarship. HJ gratefully acknowledges support from the Alexander-von-Humboldt (AvH) Foundation. HHH, JTM and KR acknowledge support from the German Research Foundation (DFG) through DFG CoE e-conversion EXC 2089/1. IB, DPK, XRA, WJB, FDP, RE, VK, DK, GL, NON, LLS, CSc, TKS, CvdO, EVU, WCW acknowledge access to CSD3 GPU resources through a University of Cambridge EPSRC Core Equipment Award (EP/X034712/1). We acknowledge project/application support by the Max Planck Computing and Data Facility. KH, JK and VS acknowledge the Swedish Research Council (Vetenskapsrådet, project number 2021-06757) and the National Strategic e-Science program eSSENCE for funding, as well as the Swedish National Infrastructure for Computing (SNIC/NAISS) for providing computer resources used in this project. SW, AB and TV acknowledge the Pioneer Center for Accelerating P2X Materials discovery (CAPeX), DNRF Grant number P3. YW acknowledges support from the Shanghai Jiao Tong University. WCW acknowledges support from the EPSRC (Grant EP/V062654/1). CO acknowledges support from NSERC (Discovery Grant GR019381) and NFRF (Exploration Grant GR022937). JG and AN would like to acknowledge the Gauss Centre for Supercomputing e.V. (https://www.gauss-centre.eu) for funding workflow-related developments by providing generous computing time on the GCS Supercomputer SuperMUC-NG at Leibniz Supercomputing Centre (www.lrz.de) (Project pn73da). SH and JJ acknowledge funding from EPSRC (EP/T001038/1, EP/S022953/1). ADK acknowledges the Savio computational cluster resource provided by the Berkeley Research Computing program at the University of California, Berkeley (supported by the UC Berkeley Chancellor, Vice Chancellor for Research, and Chief Information Officer). ACF acknowledges funding from EU Graphene Flagship, ERC grants Hetero2D, GIPT, EU grants Graph-X, CHARM, EPSRC grants EP/K01711X/1, EP/K017144/1, EP/N010345/1, EP/L016087/1, EP/V000055/1, EP/X015742/1. WB, CSu, and CG thank the US AFRL for partial funding of this project through grant FA8655-21-1-7010. GC is grateful to Ágnes Borszéki for help with graphics.

References

1. W. Kohn and L. J. Sham, "Self-consistent equations including exchange and correlation effects," *Phys. Rev.*, vol. 140, pp. A1133–A1138, Nov 1965.

2. P. Giannozzi, O. Baseggio, P. Bonfà, D. Brunato, R. Car, I. Carnimeo, C. Cavazzoni, S. de Gironcoli, P. Delugas, F. Ferrari Ruffino, A. Ferretti, N. Marzari, I. Timrov, A. Urru, and S. Baroni, "Quantum ESPRESSO toward the exascale," *The Journal of Chemical Physics*, vol. 152, p. 154105, 04 2020.

3. T. D. Kühne, M. Iannuzzi, M. Del Ben, V. V. Rybkin, P. Seewald, F. Stein, T. Laino, R. Z. Khaliullin, O. Schütt, F. Schiffmann, *et al.*, "Cp2k: An electronic structure and molecular dynamics software package-quickstep: Efficient and accurate electronic structure calculations," *The Journal of Chemical Physics*, vol. 152, no. 19, 2020.

4. G. Kresse and J. Hafner, "Ab initio molecular dynamics for liquid metals," *Phys. Rev. B*, vol. 47, p. 558, 1993.

5. P. J. Hasnip, K. Refson, M. I. J. Probert, J. R. Yates, S. J. Clark, and C. J. Pickard, "Density functional theory in the solid state," *Phil. Trans. R. Soc. A.*, vol. 372, p. 20130270, 2014.

6. A. Jain, Y. Shin, and K. A. Persson, "Computational predictions of energy materials using density functional theory," *Nat Rev Mater*, vol. 1, p. 714, 2016.

7. J. Neugebauer and T. Hickel, "Density functional theory in materials science," *WIREs Comput Mol Sci*, vol. 3, pp. 438–448, 2013.

8. M. Finnis, *Interatomic forces in condensed matter*, vol. 1. Oxford Series on Materials Mod, 2003.

9. J. Behler and M. Parrinello, "Generalized neural-network representation of high-dimensional potential-energy surfaces," *Phys. Rev. Lett.*, vol. 98, p. 146401, Apr 2007.

10. A. P. Bartók, M. C. Payne, R. Kondor, and G. Csányi, "Gaussian approximation potentials: The accuracy of quantum mechanics, without the electrons," *Phys. Rev. Lett.*, vol. 104, p. 136403, Apr 2010.

11. A. Thompson, L. Swiler, C. Trott, S. Foiles, and G. Tucker, "Spectral neighbor analysis method for automated generation of quantum-accurate interatomic potentials," *Journal of Computational Physics*, vol. 285, pp. 316–330, 2015.

12. K. T. Schütt, H. E. Sauceda, P.-J. Kindermans, A. Tkatchenko, and K.-R. Müller, "SchNet – A deep learning architecture for molecules and materials," *The Journal of Chemical Physics*, vol. 148, p. 241722, 03 2018.

13. V. L. Deringer, M. A. Caro, and G. Csányi, "Machine Learning Interatomic Potentials as Emerging Tools for Materials Science," *Advanced Materials*, vol. 31, no. 46, p. 1902765, 2019.

14. R. Drautz, "Atomic cluster expansion for accurate and transferable interatomic potentials," *Phys. Rev. B*, vol. 99, p. 014104, Jan 2019.

15. O. A. von Lilienfeld and K. Burke, "Retrospective on a decade of machine learning for chemical discovery," *Nature Communications*, vol. 11, no. 1, p. 4895, 2020.

16. S. Batzner, A. Musaelian, L. Sun, M. Geiger, J. P. Mailoa, M. Kornbluth, N. Molinari, T. E. Smidt, and B. Kozinsky, "E (3)-equivariant graph neural networks for data-efficient and accurate interatomic potentials," *Nature communications*, vol. 13, no. 1, p. 2453, 2022.

17. T. W. Ko and S. P. Ong, "Recent advances and outstanding challenges for machine learning interatomic potentials," *Nature Computational Science*, pp. 1–3, 2023.

18. V. L. Deringer, A. P. Bartók, N. Bernstein, D. M. Wilkins, M. Ceriotti, and G. Csányi, "Gaussian process regression for materials and molecules," *Chemical Reviews*, vol. 121, no. 16, pp. 10073–10141, 2021. PMID: 34398616.

19. A. Jain, S. P. Ong, G. Hautier, W. Chen, W. D. Richards, S. Dacek, S. Cholia, D. Gunter, D. Skinner, G. Ceder, *et al.*, "Commentary: The materials project: A materials genome approach to accelerating materials innovation," *APL materials*, vol. 1, no. 1, 2013.

20. S. Stocker, J. Gasteiger, F. Becker, S. Günnemann, and J. T. Margraf, "How robust are modern graph neural network potentials in long and hot molecular dynamics simulations?," *Mach. Learn.: Sci. Technol.*, vol. 3, p. 045010, 2022.

21. C. Chen, W. Ye, Y. Zuo, C. Zheng, and S. P. Ong, "Graph networks as a universal machine learning framework for molecules and crystals," *Chemistry of Materials*, vol. 31, no. 9, pp. 3564–3572, 2019.

22. J. P. Perdew, K. Burke, and M. Ernzerhof, "Generalized gradient approximation made simple," *Physical review letters*, vol. 77, no. 18, p. 3865, 1996.

23. C. Chen and S. P. Ong, "A universal graph deep learning interatomic potential for the periodic table," *Nat Comput Sci*, vol. 2, no. 11, pp. 718–728, 2022. Number: 11 Publisher: Nature Publishing Group.

24. B. Deng, P. Zhong, K. Jun, J. Riebesell, K. Han, C. J. Bartel, and G. Ceder, "CHGNet as a pre-trained universal neural network potential for charge-informed atomistic modeling," *Nature Machine Intelligence*, vol. 5, no. 9, pp. 1031–1041, 2023.

25. K. Choudhary, B. DeCost, L. Major, K. Butler, J. Thiyagalingam, and F. Tavazza, "Unified graph neural network force-field for the periodic table: solid state applications," *Digital Discovery*, vol. 2, no. 2, pp. 346–355, 2023.

26. K. Choudhary, K. F. Garrity, A. C. E. Reid, B. DeCost, A. J. Biacchi, A. R. Hight Walker, Z. Trautt, J. Hattrick-Simpers, A. G. Kusne, A. Centrone, A. Davydov, J. Jiang, R. Pachter, G. Cheon, E. Reed, A. Agrawal, X. Qian, V. Sharma, H. Zhuang, S. V. Kalinin, B. G. Sumpter, G. Pilania, P. Acar, S. Mandal, K. Haule, D. Vanderbilt, K. Rabe, and F. Tavazza, "The joint automated repository for various integrated simulations (jarvis) for data-driven materials design," *npj Computational Materials*, vol. 6, no. 1, p. 173, 2020.

27. J. Klimeš, D. R. Bowler, and A. Michaelides, "Chemical accuracy for the van der waals density functional," *Journal of Physics: Condensed Matter*, vol. 22, no. 2, p. 022201, 2010.

28. A. Merchant, S. Batzner, S. S. Schoenholz, M. Aykol, G. Cheon, and E. D. Cubuk, "Scaling deep learning for materials discovery," *Nature*, pp. 1–6, 2023. Publisher: Nature Publishing Group.

29. S. Takamoto, C. Shinagawa, D. Motoki, K. Nakago, W. Li, I. Kurata, T. Watanabe, Y. Yayama, H. Iriguchi, Y. Asano, *et al.*, "Towards universal neural network potential for material discovery applicable to arbitrary combination of 45 elements," *Nature Communications*, vol. 13, no. 1, p. 2991, 2022.

30. S. Takamoto, S. Izumi, and J. Li, "Teanet: Universal neural network interatomic potential inspired by iterative electronic relaxations," *Computational Materials Science*, vol. 207, p. 111280, 2022.

31. J. S. Smith, O. Isayev, and A. E. Roitberg, "ANI-1: an extensible neural network potential with DFT accuracy at force field computational cost," *Chem. Sci.*, vol. 8, no. 4, pp. 3192–3203, 2017. Publisher: The Royal Society of Chemistry.

32. J. S. Smith, B. T. Nebgen, R. Zubatyuk, N. Lubbers, C. Devereux, K. Barros, S. Tretiak, O. Isayev, and A. E. Roitberg, "Approaching coupled cluster accuracy with a general-purpose neural network potential through transfer learning," *Nat. Commun.*, vol. 10, no. 1, p. 2903, 2019.

33. R. Zubatyuk, J. S. Smith, J. Leszczynski, and O. Isayev, "Accurate and transferable multitask prediction of chemical properties with an atoms-in-molecules neural network," *Science Advances*, vol. 5, no. 8, p. eaav6490, 2019.

34. N. Lopanitsyna, G. Fraux, M. A. Springer, S. De, and M. Ceriotti, "Modeling high-entropy transition metal alloys with alchemical compression," *Physical Review Materials*, vol. 7, no. 4, p. 045802, 2023.

35. I. Batatia, D. P. Kovacs, G. Simm, C. Ortner, and G. Csányi, "Mace: Higher order equivariant message passing neural networks for fast and accurate force fields," *Advances in Neural Information Processing Systems*, vol. 35, pp. 11423–11436, 2022.

36. I. Batatia, S. Batzner, D. P. Kovács, A. Musaelian, G. N. C. Simm, R. Drautz, C. Ortner, B. Kozinsky, and G. Csányi, "The design space of e(3)-equivariant atom-centered interatomic potentials," 2022.

37. J. P. Darby, D. P. Kovács, I. Batatia, M. A. Caro, G. L. W. Hart, C. Ortner, and G. Csányi, "Tensor-reduced atomic density representations," *Phys. Rev. Lett.*, vol. 131, p. 028001, Jul 2023.

38. L. B. Skinner, C. Huang, D. Schlesinger, L. G. M. Pettersson, A. Nilsson, and C. J. Benmore, "Benchmark oxygen-oxygen pair-distribution function of ambient water from x-ray diffraction measurements with a wide Q-range," *J. Chem. Phys.*, vol. 138, p. 074506, 02 2013.

39. J. E. Bertie and Z. Lan, "Infrared intensities of liquids xx: The intensity of the OH stretching band of liquid water revisited, and the best current values of the optical constants of H_2O(l) at 25°c between 15,000 and 1 cm^{-1}," *Appl. Spectrosc.*, vol. 50, no. 8, pp. 1047–1057, 1996.

40. D. R. Moberg, S. C. Straight, C. Knight, and F. Paesani, "Molecular Origin of the Vibrational Structure of Ice Ih," *J. Phys. Chem. Lett.*, vol. 8, no. 12, pp. 2579–2583, 2017. PMID: 28541703.

41. S. Grimme, J. Antony, S. Ehrlich, and H. Krieg, "A consistent and accurate ab initio parametrization of density functional dispersion correction (dft-d) for the 94 elements h-pu," *The Journal of chemical physics*, vol. 132, no. 15, 2010.

42. N. O'Neill, C. Schran, S. J. Cox, and A. Michaelides, "Crumbling crystals: On the dissolution mechanism of nacl in water," 2022.

43. M. J. Gillan, D. Alfe, and A. Michaelides, "Perspective: How good is dft for water?," *The Journal of chemical physics*, vol. 144, no. 13, 2016.

44. D. Marx, M. E. Tuckerman, J. Hutter, and M. Parrinello, "The nature of the hydrated excess proton in water," *Nature*, vol. 397, pp. 601–604, feb 1999.

45. M. E. Tuckerman, D. Marx, and M. Parrinello, "The nature and transport mechanism of hydrated hydroxide ions in aqueous solution," *Nature*, vol. 417, pp. 925–929, jun 2002.

46. N. Agmon, H. J. Bakker, R. K. Campen, R. H. Henchman, P. Pohl, S. Roke, M. Thämer, and A. Hassanali, "Protons and Hydroxide Ions in Aqueous Systems," *Chem. Rev.*, vol. 116, pp. 7642–7672, jul 2016.

47. F. Della Pia, A. Zen, D. Alfè, and A. Michaelides, "DMC-ICE13: Ambient and high pressure polymorphs of ice from diffusion Monte Carlo and density functional theory," *The Journal of Chemical Physics*, vol. 157, p. 134701, 10 2022.

48. G. Algara-Siller, O. Lehtinen, F. C. Wang, R. R. Nair, U. Kaiser, H. A. Wu, A. K. Geim, and I. V. Grigorieva, "Square ice in graphene nanocapillaries," *Nature*, vol. 519, pp. 443–445, mar 2015.

49. L. Fumagalli, A. Esfandiar, R. Fabregas, S. Hu, P. Ares, A. Janardanan, Q. Yang, B. Radha, T. Taniguchi, K. Watanabe, G. Gomila, K. S. Novoselov, and A. K. Geim, "Anomalously low dielectric constant of confined water," *Science*, vol. 360, pp. 1339–1342, jun 2018.

50. V. Kapil, C. Schran, A. Zen, J. Chen, C. J. Pickard, and A. Michaelides, "The first-principles phase diagram of monolayer nanoconfined water," *Nature*, vol. 609, no. 7927, pp. 512–516, 2022.

51. H. A. Hansen, J. Rossmeisl, and J. K. Nørskov, "Surface pourbaix diagrams and oxygen reduction activity of Pt, Ag and Ni(111) surfaces studied by DFT," *Phys. Chem. Chem. Phys.*, vol. 10, pp. 3722–3730, July 2008.

52. S. Vijay, G. Kastlunger, K. Chan, and J. K. Nørskov, "Limits to scaling relations between adsorption energies?," *The Journal of Chemical Physics*, vol. 156, June 2022.

53. A. Tiwari, H. H. Heenen, A. S. Bjørnlund, D. Hochfilzer, K. Chan, and S. Horch, "Electrochemical oxidation of co on cu single crystals under alkaline conditions," *ACS Energy Letters*, vol. 5, no. 11, pp. 3437–3442, 2020.

54. L. L. Schaaf, E. Fako, S. De, A. Schäfer, and G. Csányi, "Accurate energy barriers for catalytic reaction pathways: an automatic training protocol for machine learning force fields," *npj Computational Materials*, vol. 9, no. 1, p. 180, 2023.

55. L. McInnes, J. Healy, and J. Melville, "Umap: Uniform manifold approximation and projection for dimension reduction," *arXiv preprint arXiv:1802.03426*, 2018.

56. R. Elijošius, "MACE-MP UMAP analysis," *github.com*, 2023. 10.5281/zenodo.10426282 - https://github.com/RokasEl/mace-mp-umap.

57. J. K. Nørskov, T. Bligaard, J. Rossmeisl, and C. H. Christensen, "Towards the computational design of solid catalysts," *Nature Chem*, vol. 1, pp. 37–46, 2009.

58. A. J. Medford, A. Vojvodic, J. S. Hummelshøj, J. Voss, F. Abild-pedersen, F. Studt, T. Bligaard, A. Nilsson, and J. K. Nørskov, "From the sabatier principle to a predictive theory of transition-metal heterogeneous catalysis," *Journal of Catalysis*, vol. 328, pp. 36–42, 2015.

59. A. Bruix, J. T. Margraf, M. Andersen, and K. Reuter, "First-principles-based multiscale modelling of heterogeneous catalysis," *Nat Catal*, vol. 2, pp. 659–670, 2019.

60. X. Qin, T. Vegge, and H. A. Hansen, "Cation-coordinated inner-sphere co₂electroreduction at au–water interfaces," *J. Am. Chem. Soc.*, vol. 145, pp. 1897–1905, 2023.

61. I. C. Man, H. Su, F. Calle-vallejo, H. A. Hansen, J. I. Martínez, N. G. Inoglu, J. Kitchin, T. F. Jaramillo, J. K. Nørskov, and J. Rossmeisl, "Universality in oxygen evolution electrocatalysis on oxide surfaces," *ChemCatChem*, vol. 3, pp. 1159–1165, 2011.

62. A. Auer, M. Andersen, E.-M. Wernig, N. G. Hörmann, N. Buller, K. Reuter, and J. Kunze-liebhäuser, "Self-activation of copper electrodes during co electro-oxidation in alkaline electrolyte," *Nat Catal*, vol. 3, pp. 797–803, 2020.

63. Q. Wang, J. Pan, J. Guo, H. A. Hansen, H. Xie, L. Jiang, L. Hua, H. Li, Y. Guan, P. Wang, W. Gao, L. Liu, H. Cao, Z. Xiong, T. Vegge, and P. Chen, "Ternary ruthenium complex hydrides for ammonia synthesis via the associative mechanism," *Nat Catal*, vol. 4, pp. 959–967, 2021.

64. J. K. Nørskov, F. Studt, F. Abild-Pedersen, and T. Bligaard, *Fundamental Concepts in Heterogeneous Catalysis*. John Wiley & Sons, Inc., 2014.

65. J. T. Margraf, H. Jung, C. Scheurer, and K. Reuter, "Exploring catalytic reaction networks with machine learning," *Nat Catal*, vol. 6, pp. 112–121, 2023.

66. X. Yang, A. Bhowmik, T. Vegge, and H. A. Hansen, "Neural network potentials for accelerated meta-dynamics of oxygen reduction kinetics at au–water interfaces," *Chem. Sci.*, vol. 14, pp. 3913–3922, 2023.

67. K. Tran and Z. W. Ulissi, "Active learning across intermetallics to guide discovery of electrocatalysts for co2 reduction and h2 evolution," *Nat Catal*, vol. 1, pp. 696–703, 2018.

68. L. Foppa, C. Sutton, L. M. Ghiringhelli, S. De, P. Löser, S. A. Schunk, A. Schäfer, and M. Scheffler, "Learning design rules for selective oxidation catalysts from high-throughput experimentation and artificial intelligence," *ACS Catalysis*, vol. 12, no. 4, pp. 2223–2232, 2022.

69. M. Khatamirad, E. Fako, C. Boscagli, M. Müller, F. Ebert, R. Naumann d'Alnoncourt, A. Schaefer, S. A. Schunk, I. Jevtovikj, F. Rosowski, and S. De, "A data-driven high-throughput workflow applied to promoted in-oxide catalysts for co2 hydrogenation to methanol," *Catalysis Science & Technology*, vol. 13, no. 9, p. 2656–2661, 2023.

70. S. Stocker, H. Jung, G. Csányi, C. F. Goldsmith, K. Reuter, and J. T. Margraf, "Estimating free energy barriers for heterogeneous catalytic reactions with machine learning potentials and umbrella integration," *J. Chem. Theory Comput.*, vol. 19, pp. 6796–6804, 2023.

71. R. Tran, J. Lan, M. Shuaibi, B. M. Wood, S. Goyal, A. Das, J. Heras-domingo, A. Kolluru, A. Rizvi, N. Shoghi, A. Sriram, F. Therrien, J. Abed, O. Voznyy, E. H. Sargent, Z. Ulissi, and C. L. Zitnick, "The open catalyst 2022 (oc22) dataset and challenges for oxide electrocatalysts," *ACS Catal.*, vol. 13, pp. 3066–3084, 2023.

72. M. Pourbaix, *ATLAS of Electrochemical Equilibria in Aqueous Solutions*. Pergamon Press, Oxford, 1966.

73. M. Pourbaix, *Lectures on Electrochemical Corrosion*. Springer Science and Business Media, 1973.

74. J. K. Nørskov, J. Rossmeisl, A. Logadottir, L. Lindqvist, J. R. Kitchin, T. Bligaard, and H. Jónsson, "Origin of the overpotential for oxygen reduction at a fuel-cell cathode," *J. Phys. Chem. B*, vol. 108, pp. 17886–17892, Nov. 2004.

75. K. A. Persson, B. Waldwick, P. Lazic, and G. Ceder, "Prediction of solid-aqueous equilibria: Scheme to combine first-principles calculations of solids with experimental aqueous states," *Phys. Rev. B Condens. Matter Mater. Phys.*, vol. 85, June 2012.

76. A. K. Singh, L. Zhou, A. Shinde, S. K. Suram, J. H. Montoya, D. Winston, J. M. Gregoire, and K. A. Persson, "Electrochemical stability of metastable materials," *Chem. Mater.*, vol. 29, pp. 10159–10167, Dec. 2017.

77. F. Abild-Pedersen, J. Greeley, F. Studt, J. Rossmeisl, T. R. Munter, P. G. Moses, E. Skúlason, T. Bligaard, and J. K. Nørskov, "Scaling properties of adsorption energies for hydrogen-containing molecules on transition-metal surfaces," *Physical Review Letters*, vol. 99, July 2007.

78. J. Pérez-Ramírez and N. López, "Strategies to break linear scaling relationships," *Nature Catalysis*, vol. 2, p. 971–976, Oct. 2019.

79. R. García-Muelas and N. López, "Statistical learning goes beyond the d-band model providing the thermochemistry of adsorbates on transition metals," *Nat. Commun.*, vol. 10, p. 4687, Oct. 2019.

80. S. Dang, B. Qin, Y. Yang, H. Wang, J. Cai, Y. Han, S. Li, P. Gao, and Y. Sun, "Rationally designed indium oxide catalysts for CO_2 hydrogenation to methanol with high activity and selectivity," *Science advances*, vol. 6, no. 25, p. eaaz2060, 2020.

81. A. S. Rosen, S. M. Iyer, D. Ray, Z. Yao, A. Aspuru-Guzik, L. Gagliardi, J. M. Notestein, and R. Q. Snurr, "Machine learning the quantum-chemical properties of metal–organic frameworks for accelerated materials discovery," *Matter*, vol. 4, no. 5, pp. 1578–1597, 2021.

82. A. S. Rosen, V. Fung, P. Huck, C. T. O'Donnell, M. K. Horton, D. G. Truhlar, K. A. Persson, J. M. Notestein, and R. Q. Snurr, "High-throughput predictions of metal–organic framework electronic properties: theoretical challenges, graph neural networks, and data exploration," *npj Computational Materials*, vol. 8, no. 1, p. 112, 2022.

83. J. Zeng, D. Zhang, D. Lu, P. Mo, Z. Li, Y. Chen, M. Rynik, L. Huang, Z. Li, S. Shi, Y. Wang, H. Ye, P. Tuo, J. Yang, Y. Ding, Y. Li, D. Tisi, Q. Zeng, H. Bao, Y. Xia, J. Huang, K. Muraoka, Y. Wang, J. Chang, F. Yuan, S. L. Bore, C. Cai, Y. Lin, B. Wang, J. Xu, J.-X. Zhu, C. Luo, Y. Zhang, R. E. A. Goodall, W. Liang, A. K. Singh, S. Yao, J. Zhang, R. Wentzcovitch, J. Han, J. Liu, W. Jia, D. M. York, W. E, R. Car, L. Zhang, and H. Wang, "DeePMD-kit v2: A software package for deep potential models," *The Journal of Chemical Physics*, vol. 159, p. 054801, 08 2023.

84. A. K. Rappé, C. J. Casewit, K. Colwell, W. A. Goddard III, and W. M. Skiff, "Uff, a full periodic table force field for molecular mechanics and molecular dynamics simulations," *Journal of the American chemical society*, vol. 114, no. 25, pp. 10024–10035, 1992.

85. T. A. Manz and N. G. Limas, "Introducing ddec6 atomic population analysis: part 1. charge partitioning theory and methodology," *RSC advances*, vol. 6, no. 53, pp. 47771–47801, 2016.

86. J. J. Potoff and J. I. Siepmann, "Vapor–liquid equilibria of mixtures containing alkanes, carbon dioxide, and nitrogen," *AIChE journal*, vol. 47, no. 7, pp. 1676–1682, 2001.

87. O. M. Yaghi, M. J. Kalmutzki, and C. S. Diercks, *Introduction to reticular chemistry: metal-organic frameworks and covalent organic frameworks*. John Wiley & Sons, 2019.

88. D. Britt, H. Furukawa, B. Wang, T. G. Glover, and O. M. Yaghi, "Highly efficient separation of carbon dioxide by a metal-organic framework replete with open metal sites," *Proceedings of the National Academy of Sciences*, vol. 106, no. 49, pp. 20637–20640, 2009.

89. W. L. Queen, M. R. Hudson, E. D. Bloch, J. A. Mason, M. I. Gonzalez, J. S. Lee, D. Gygi, J. D. Howe, K. Lee, T. A. Darwish, *et al.*, "Comprehensive study of carbon dioxide adsorption in the metal–organic frameworks M 2 (dobdc)(M= Mg, Mn, Fe, Co, Ni, Cu, Zn)," *Chemical Science*, vol. 5, no. 12, pp. 4569–4581, 2014.

90. J. H. Choe, H. Kim, and C. S. Hong, "Mof-74 type variants for co 2 capture," *Materials Chemistry Frontiers*, vol. 5, no. 14, pp. 5172–5185, 2021.

91. Ü. Kökçam-Demir, A. Goldman, L. Esrafili, M. Gharib, A. Morsali, O. Weingart, and C. Janiak, "Coordinatively unsaturated metal sites (open metal sites) in metal–organic frameworks: design and applications," *Chemical Society Reviews*, vol. 49, no. 9, pp. 2751–2798, 2020.

92. B. Zheng, F. L. Oliveira, R. Neumann Barros Ferreira, M. Steiner, H. Hamann, G. X. Gu, and B. Luan, "Quantum informed machine-learning potentials for molecular dynamics simulations of CO_2's chemisorption and diffusion in Mg-MOF-74," *ACS nano*, vol. 17, no. 6, pp. 5579–5587, 2023.

93. L. Valenzano, B. Civalleri, S. Chavan, G. T. Palomino, C. O. Areán, and S. Bordiga, "Computational and experimental studies on the adsorption of CO, N_2, and CO_2 on Mg-MOF-74," *The Journal of Physical Chemistry C*, vol. 114, no. 25, pp. 11185–11191, 2010.

94. M. Witman, S. Ling, S. Anderson, L. Tong, K. C. Stylianou, B. Slater, B. Smit, and M. Haranczyk, "In silico design and screening of hypothetical mof-74 analogs and their experimental synthesis," *Chemical science*, vol. 7, no. 9, pp. 6263–6272, 2016.

95. T. D. Bennett and S. Horike, "Liquid, glass and amorphous solid states of coordination polymers and metal–organic frameworks," *Nature Reviews Materials*, vol. 3, no. 11, pp. 431–440, 2018.

96. N. Castel and F.-X. Coudert, "Atomistic Models of Amorphous Metal–Organic Frameworks," *The Journal of Physical Chemistry C*, vol. 126, no. 16, pp. 6905–6914, 2022.

97. J. D. Evans, V. Bon, I. Senkovska, H.-C. Lee, and S. Kaskel, "Four-dimensional metal-organic frameworks," *Nature Communications*, vol. 11, no. 1, p. 2690, 2020.

98. M. K. Taylor, T. Runcevski, J. Oktawiec, J. E. Bachman, R. L. Siegelman, H. Jiang, J. A. Mason, J. D. Tarver, and J. R. Long, "Near-perfect CO_2/CH_4 selectivity achieved through reversible guest templating in the flexible metal–organic framework co (bdp)," *Journal of the American Chemical Society*, vol. 140, no. 32, pp. 10324–10331, 2018.

99. V. Van Speybroeck, S. Vandenhaute, A. E. Hoffman, and S. M. Rogge, "Towards modeling spatiotemporal processes in metal–organic frameworks," *Trends Chem.*, vol. 3, pp. 605–619, 2021.

100. J. Řezáč, K. E. Riley, and P. Hobza, "S66: A well-balanced database of benchmark interaction energies relevant to biomolecular structures," *Journal of Chemical Theory and Computation*, vol. 7, no. 8, pp. 2427–2438, 2011. PMID: 21836824.

101. A. M. Reilly and A. Tkatchenko, "Understanding the role of vibrations, exact exchange, and many-body van der Waals interactions in the cohesive properties of molecular crystals," *The Journal of Chemical Physics*, vol. 139, p. 024705, 07 2013.

102. T. W. Keal and D. J. Tozer, "Semiempirical hybrid functional with improved performance in an extensive chemical assessment," *The Journal of Chemical Physics*, vol. 123, p. 121103, 09 2005.

103. J. W. Furness, A. D. Kaplan, J. Ning, J. P. Perdew, and J. Sun, "Accurate and numerically efficient r^{2}SCAN meta-generalized gradient approximation," *J. Phys. Chem. Lett.*, vol. 11, pp. 8208–8215, 2020.

104. R. Kingsbury, A. S. Gupta, C. J. Bartel, J. M. Munro, S. Dwaraknath, M. Horton, and K. A. Persson, "Performance comparison of r^{2}SCAN and SCAN metaGGA density functionals for solid materials via an automated, high-throughput computational workflow," *Phys. Rev. Materials*, vol. 6, 2022.

105. T. M. Henderson, J. Paier, and G. E. Scuseria, "Accurate treatment of solids with the HSE screened hybrid," *physica status solidi (b)*, vol. 248, no. 4, pp. 767–774, 2011.

106. J. Harl, L. Schimka, and G. Kresse, "Assessing the quality of the random phase approximation for lattice constants and atomization energies of solids," *Phys. Rev. B*, vol. 81, p. 115126, Mar. 2010.

107. S. A. Ghasemi, A. Hofstetter, S. Saha, and S. Goedecker, "Interatomic potentials for ionic systems with density functional accuracy based on charge densities obtained by a neural network," *Phys. Rev. B*, vol. 92, 2015.

108. A. Grisafi and M. Ceriotti, "Incorporating long-range physics in atomic-scale machine learning," *J. Chem. Phys.*, vol. 151, p. 12828, 2019.

109. T. W. Ko, J. A. Finkler, S. Goedecker, and J. Behler, "A fourth-generation high-dimensional neural network potential with accurate electrostatics including non-local charge transfer," *Nat Commun*, vol. 12, p. 585, 2021.

110. M. Vondrák, K. Reuter, and J. T. Margraf, "q-pac: A python package for machine learned charge equilibration models," *J. Chem. Phys.*, vol. 159, p. 10037, 2023.

111. I. Novikov, B. Grabowski, F. Körmann, and A. Shapeev, "Magnetic moment tensor potentials for collinear spin-polarized materials reproduce different magnetic states of bcc fe," *npj Computational Materials*, vol. 8, no. 1, p. 13, 2022.

112. M. Rinaldi, M. Mrovec, A. Bochkarev, Y. Lysogorskiy, and R. Drautz, "Non-collinear magnetic atomic cluster expansion for iron," 2023.

113. I.-B. Magdău, D. J. Arismendi-Arrieta, H. E. Smith, C. P. Grey, K. Hermansson, and G. Csányi, "Machine learning force fields for molecular liquids: Ethylene carbonate/ethyl methyl carbonate binary solvent," *npj Computational Materials*, vol. 9, no. 1, p. 146, 2023.

114. J. Byggmästar, A. Hamedani, K. Nordlund, and F. Djurabekova, "Machine-learning interatomic potential for radiation damage and defects in tungsten," *Phys. Rev. B*, vol. 100, p. 144105, Oct 2019.

115. J. D. Morrow, J. L. A. Gardner, and V. L. Deringer, "How to validate machine-learned interatomic potentials," *J. Chem. Phys.*, vol. 158, p. 121501, Mar. 2023.

116. J. L. A. Gardner, K. T. Baker, and V. L. Deringer, "Synthetic pre-training for neural-network interatomic potentials," *Mach. Learn.: Sci. Technol.*, pp. in press, DOI: 10.1088/2632–2153/ad1626, 2023.

117. A. P. Bartók, M. J. Gillan, F. R. Manby, and G. Csányi, "Machine-learning approach for one- and two-body corrections to density functional theory: Applications to molecular and condensed water," *Phys. Rev. B*, vol. 88, p. 054104, Aug 2013.

118. P. O. Dral, A. Owens, A. Dral, and G. Csányi, "Hierarchical machine learning of potential energy surfaces," *The Journal of Chemical Physics*, vol. 152, p. 204110, 05 2020.

119. A. Paszke, S. Gross, F. Massa, A. Lerer, J. Bradbury, G. Chanan, T. Killeen, Z. Lin, N. Gimelshein, L. Antiga, A. Desmaison, A. Köpf, E. Yang, Z. DeVito, M. Raison, A. Tejani, S. Chilamkurthy, B. Steiner, L. Fang, J. Bai, and S. Chintala, "Pytorch: An imperative style, high-performance deep learning library," in *Neural Information Processing Systems*, 2019.

120. M. Geiger and T. Smidt, "e3nn: Euclidean neural networks," 2022.

121. D. P. Kovács, I. Batatia, E. S. Arany, and G. Csányi, "Evaluation of the MACE force field architecture: From medicinal chemistry to materials science," *The Journal of Chemical Physics*, vol. 159, p. 044118, 07 2023.

122. S. J. Reddi, S. Kale, and S. Kumar, "On the convergence of adam and beyond," *arXiv preprint arXiv:1904.09237*, 2019.

123. D. P. Kingma and J. Ba, "Adam: A method for stochastic optimization," *arXiv preprint arXiv:1412.6980*, 2014.

124. "Materials project calculation details." https://docs.materialsproject.org/methodology/materials-methodology/calculation-details. Accessed: 2023-12-18.

125. "Materials project." https://docs.materialsproject.org/methodology/materials-methodology/calculation-details/gga+u-calculations/hubbard-u-values. Accessed: 2023-12-12.

126. A. Jain, G. Hautier, S. P. Ong, C. J. Moore, C. C. Fischer, K. A. Persson, and G. Ceder, "Formation enthalpies by mixing GGA and GGA + *U* calculations," *Phys. Rev. B*, vol. 84, p. 045115, July 2011.

127. M. K. Horton, J. H. Montoya, M. Liu, and K. A. Persson, "High-throughput prediction of the ground-state collinear magnetic order of inorganic materials using Density Functional Theory," *npj Comput Mater*, vol. 5, pp. 1–11, June 2019.

128. R. Sabatini, T. Gorni, and S. de Gironcoli, "Nonlocal van der waals density functional made simple and efficient," *Phys. Rev. B*, vol. 87, p. 041108, Jan 2013.

129. I.-C. Lin, A. P. Seitsonen, I. Tavernelli, and U. Rothlisberger, "Structure and dynamics of liquid water from ab initio molecular dynamics—comparison of blyp, pbe, and revpbe density functionals with and without van der waals corrections," *J. Chem. Theory Comput.*, vol. 8, no. 10, pp. 3902–3910, 2012.

130. A. V. Terentjev, L. A. Constantin, and J. M. Pitarke, "Dispersion-corrected pbesol exchange-correlation functional," *Phys. Rev. B*, vol. 98, p. 214108, Dec 2018.

131. F. Formalik, M. Fischer, J. Rogacka, L. Firlej, and B. Kuchta, "Benchmarking of GGA density functionals for modeling structures of nanoporous, rigid and flexible MOFs," *J. Chem. Phys.*, vol. 149, p. 064110, 08 2018.

132. B. M. Axilrod and E. Teller, "Interaction of the van der Waals Type Between Three Atoms," *J. Chem. Phys.*, vol. 11, pp. 299–300, 12 2004.

133. S. Grimme, S. Ehrlich, and L. Goerigk, "Effect of the damping function in dispersion corrected density functional theory," *Journal of computational chemistry*, vol. 32, no. 7, pp. 1456–1465, 2011.

134. A. P. Bartók, J. Kermode, N. Bernstein, and G. Csányi, "Machine learning a general-purpose interatomic potential for silicon," *Physical Review X*, vol. 8, no. 4, p. 041048, 2018.

135. Y. Yoshida and G. Langouche, *Defects and Impurities in Silicon Materials*. Springer, 2015.

136. D. Richie, J. Kim, S. A. Barr, K. R. Hazzard, R. Hennig, and J. W. Wilkins, "Complexity of small silicon self-interstitial defects," *Physical review letters*, vol. 92, no. 4, p. 045501, 2004.

137. B. Sahli and W. Fichtner, "Ab initio molecular dynamics simulation of self-interstitial diffusion in silicon," *Physical Review B*, vol. 72, no. 24, p. 245210, 2005.

138. M. Posselt, F. Gao, and D. Zwicker, "Migration of di-and tri-interstitials in silicon," *Nuclear Instruments and Methods in Physics Research Section B: Beam Interactions with Materials and Atoms*, vol. 228, no. 1-4, pp. 212–217, 2005.

139. Y. A. Du, S. A. Barr, K. R. Hazzard, T. J. Lenosky, R. G. Hennig, and J. W. Wilkins, "Fast diffusion mechanism of silicon tri-interstitial defects," *Physical Review B*, vol. 72, no. 24, p. 241306, 2005.

140. P. Pichler, *Intrinsic point defects, impurities, and their diffusion in silicon*. Springer Science & Business Media, 2012.

141. F. Dorner, Z. Sukurma, C. Dellago, and G. Kresse, "Melting si: beyond density functional theory," *Physical Review Letters*, vol. 121, no. 19, p. 195701, 2018.

142. V. L. Deringer, N. Bernstein, G. Csányi, C. Ben Mahmoud, M. Ceriotti, M. Wilson, D. A. Drabold, and S. R. Elliott, "Origins of structural and electronic transitions in disordered silicon," *Nature*, vol. 589, no. 7840, pp. 59–64, 2021.

143. N. Bernstein, B. Bhattarai, G. Csányi, D. A. Drabold, S. R. Elliott, and V. L. Deringer, "Quantifying Chemical Structure and Machine-Learned Atomic Energies in Amorphous and Liquid Silicon," *Angew. Chem. Int. Ed.*, vol. 58, pp. 7057–7061, 2019.

144. Y. Lysogorskiy, C. v. d. Oord, A. Bochkarev, S. Menon, M. Rinaldi, T. Hammerschmidt, M. Mrovec, A. Thompson, G. Csányi, C. Ortner, *et al.*, "Performant implementation of the atomic cluster expansion (pace) and application to copper and silicon," *npj computational materials*, vol. 7, no. 1, p. 97, 2021.

145. J. D. Morrow and V. L. Deringer, "Indirect learning and physically guided validation of interatomic potential models," *J. Chem. Phys.*, vol. 157, no. 10, p. 104105, 2022.

146. V. L. Deringer, N. Bernstein, A. P. Bartók, M. J. Cliffe, R. N. Kerber, L. E. Marbella, C. P. Grey, S. R. Elliott, and G. Csányi, "Realistic atomistic structure of amorphous silicon from machine-learning-driven molecular dynamics," *The journal of physical chemistry letters*, vol. 9, no. 11, pp. 2879–2885, 2018.

147. S. Plimpton, "Fast parallel algorithms for short-range molecular dynamics," *Journal of computational physics*, vol. 117, no. 1, pp. 1–19, 1995.

148. S. Roorda, W. Sinke, J. Poate, D. Jacobson, S. Dierker, B. Dennis, D. Eaglesham, F. Spaepen, and P. Fuoss, "Structural relaxation and defect annihilation in pure amorphous silicon," *Physical review B*, vol. 44, no. 8, p. 3702, 1991.

149. P. Grigorev, L. Frérot, F. Birks, A. Gola, J. Golebiowski, J. Grießer, J. L. Hörmann, A. Klemenz, G. Moras, W. G. Nöhring, *et al.*, "matscipy: materials science at the atomic scale with python," *The Journal of Open Source Software (JOSS)*, 2023.

150. V. L. Deringer and G. Csányi, "Machine learning based interatomic potential for amorphous carbon," *Phys. Rev. B*, vol. 95, p. 094203, Mar 2017.

151. R. Jana, D. Savio, V. L. Deringer, and L. Pastewka, "Structural and elastic properties of amorphous carbon from simulated quenching at low rates," *Modeling and Simulation in Materials Science and Engineering*, vol. 27, p. 085009, Oct. 2019.

152. M. Qamar, M. Mrovec, Y. Lysogorskiy, A. Bochkarev, and R. Drautz, "Atomic cluster expansion for quantum-accurate large-scale simulations of carbon," *Journal of Chemical Theory and Computation*, vol. 19, p. 5151–5167, June 2023.

153. T. K. Stenczel, Z. El-Machachi, G. Liepuoniute, J. D. Morrow, A. P. Bartók, M. I. J. Probert, G. Csányi, and V. L. Deringer, "Machine-learned acceleration for molecular dynamics in CASTEP," *J. Chem. Phys.*, vol. 159, p. 044803, 07 2023.

154. C. de Tomas, A. Aghajamali, J. L. Jones, D. J. Lim, M. J. López, I. Suarez-Martinez, and N. A. Marks, "Transferability in interatomic potentials for carbon," *Carbon*, vol. 155, pp. 624–634, 2019.

155. G. A. Marchant, M. A. Caro, B. Karasulu, and L. B. Pártay, "Exploring the configuration space of elemental carbon with empirical and machine learned interatomic potentials," *npj Comput. Mater.*, vol. 9, p. 131, 2023.

156. M. A. Caro, V. L. Deringer, J. Koskinen, T. Laurila, and G. Csányi, "Growth mechanism and origin of high sp^3 content in tetrahedral amorphous carbon," *Phys. Rev. Lett.*, vol. 120, p. 166101, Apr 2018.

157. P. Broqvist, J. Kullgren, M. J. Wolf, A. C. van Duin, and K. Hermansson, "Reaxff force-field for ceria bulk, surfaces, and nanoparticles," *The Journal of Physical Chemistry C*, vol. 119, no. 24, pp. 13598–13609, 2015.

158. T. P. Senftle, S. Hong, M. M. Islam, S. B. Kylasa, Y. Zheng, Y. K. Shin, C. Junkermeier, R. Engel-Herbert, M. J. Janik, H. M. Aktulga, T. Verstraelen, A. Grama, and A. C. T. van Duin, "The reaxff reactive force-field: development, applications and future directions," *npj Computational Materials*, vol. 2, p. 15011, 2016.

159. J. Kullgren, K. Hermansson, and P. Broqvist, "Supercharged low-temperature oxygen storage capacity of ceria at the nanoscale," *The journal of physical chemistry letters*, vol. 4, no. 4, pp. 604–608, 2013.

160. A. Marronnier, G. Roma, S. Boyer-Richard, L. Pedesseau, J. M. Jancu, Y. Bonnassieux, C. Katan, C. C. Stoumpos, M. G. Kanatzidis, and J. Even, "Anharmonicity and disorder in the black phases of cesium lead iodide used for stable inorganic perovskite solar cells," *ACS Nano*, vol. 12, pp. 3477–3486, 4 2018.

161. W. J. Baldwin, X. Liang, J. Klarbring, M. Dubajic, D. Dell'Angelo, C. Sutton, C. Caddeo, S. D. Stranks, A. Mattoni, A. Walsh, and G. Csányi, "Dynamic local structure in caesium lead iodide: Spatial correlation and transient domains," *Small*, vol. n/a, no. n/a, p. 2303565, 2023.

162. E. Fransson, J. Wiktor, and P. Erhart, "Phase transitions in inorganic halide perovskites from machine-learned potentials," *The Journal of Physical Chemistry C*, vol. 127, no. 28, pp. 13773–13781, 2023.

163. R. Jinnouchi, J. Lahnsteiner, F. Karsai, G. Kresse, and M. Bokdam, "Phase transitions of hybrid perovskites simulated by machine-learning force fields trained on the fly with bayesian inference," *Phys. Rev. Lett.*, vol. 122, p. 225701, Jun 2019.

164. D. H. Cao, C. C. Stoumpos, O. K. Farha, J. T. Hupp, and M. G. Kanatzidis, "2d homologous perovskites as light-absorbing materials for solar cell applications," *Journal of the American Chemical Society*, vol. 137, no. 24, pp. 7843–7850, 2015. PMID: 26020457.

165. S. Agrawalla and A. C. T. van Duin, "Development and application of a reaxff reactive force field for hydrogen combustion," *The Journal of Physical Chemistry A*, vol. 115, no. 6, pp. 960–972, 2011. PMID: 21261320.

166. D. L. Baulch, C. T. Bowman, C. J. Cobos, R. A. Cox, T. Just, J. A. Kerr, M. J. Pilling, D. Stocker, J. Troe, W. Tsang, R. W. Walker, and J. Warnatz, "Evaluated Kinetic Data for Combustion Modeling: Supplement II," *Journal of Physical and Chemical Reference Data*, vol. 34, pp. 757–1397, 07 2005.

167. L. Martínez, R. Andrade, E. G. Birgin, and J. M. Martínez, "Packmol: A package for building initial configurations for molecular dynamics simulations," *Journal of computational chemistry*, vol. 30, no. 13, pp. 2157–2164, 2009.

168. A. Stukowski, "Visualization and analysis of atomistic simulation data with ovito–the open visualization tool," *Modeling and simulation in materials science and engineering*, vol. 18, no. 1, p. 015012, 2009.

169. R. Steudel, *Elemental sulfur and sulfur-rich compounds II*, vol. 2. Springer Science & Business Media, 2003.

170. P. Lindgren, G. Kastlunger, and A. A. Peterson, "Scaled and dynamic optimizations of nudged elastic bands," *Journal of Chemical Theory and Computation*, vol. 15, no. 11, p. 5787–5793, 2019. PMID: 31600078.

171. S. Makri, C. Ortner, and J. R. Kermode, "A preconditioning scheme for minimum energy path finding methods," *The Journal of Chemical Physics*, vol. 150, p. 094109, 03 2019.

172. M. Trachta, O. Bludský, J. Vaculík, R. Bulánek, and M. Rubeš, "Investigation of brønsted acidity in zeolites through adsorbates with diverse proton affinities," *Scientific Reports*, vol. 13, p. 12380, Jul 2023.

173. S. Melchionna, G. Ciccotti, and B. L. Holian, "Hoover npt dynamics for systems varying in shape and size," *Molecular Physics*, vol. 78, no. 3, pp. 533–544, 1993.

174. S. Melchionna, "Constrained systems and statistical distribution," *Phys. Rev. E*, vol. 61, pp. 6165–6170, Jun 2000.

175. C. S. Cucinotta, A. Ruini, A. Catellani, and A. Stirling, "Ab initio molecular dynamics study of the keto–enol tautomerism of acetone in solution," *ChemPhysChem*, vol. 7, no. 6, p. 1229–1234, 2006.

176. A. M. Elena, "md driver," *gitlab.com*, 2023. 10.5281/zenodo.10432005 - https://gitlab.com/drFaustroll/lavello.

177. D. A. Stevens and J. R. Dahn, "The mechanisms of lithium and sodium insertion in carbon materials," *Journal of The Electrochemical Society*, vol. 148, p. A803, jun 2001.

178. J.-X. Huang, G. Csányi, J.-B. Zhao, J. Cheng, and V. L. Deringer, "First-principles study of alkali-metal intercalation in disordered carbon anode materials," *J. Mater. Chem. A*, vol. 7, pp. 19070–19080, 2019.

179. M. Babar, H. L. Parks, G. Houchins, and V. Viswanathan, "An accurate machine learning calculator for the lithium-graphite system," *Journal of Physics: Energy*, vol. 3, p. 014005, dec 2020.

180. A. Genreith-Schriever, A. Alexiu, G. Phillips, C. Coates, L. Nagle-Cocco, J. Bocarsly, F. Sayed, S. Dutton, and C. Grey, "Jahn-Teller distortions and phase transitions in $LiNiO_2$: Insights from *ab initio* molecular dynamics and variable-temperature x-ray diffraction.," *ChemRrxiv preprint*, 2023.

181. B. Devincre, T. Hoc, and L. Kubin, "Dislocation mean free paths and strain hardening of crystals," *Science*, vol. 320, no. 5884, pp. 1745–1748, 2008.

182. P. Grigorev, D. Terentyev, V. Dubinko, G. Bonny, G. Van Oost, J.-M. Noterdaeme, and E. E. Zhurkin, "Nucleation and growth of hydrogen bubbles on dislocations in tungsten under high flux low energy plasma exposure," *Nuclear Instruments and Methods in Physics Research Section B: Beam Interactions with Materials and Atoms*, vol. 352, pp. 96–99, 2015.

183. J. Chang, W. Cai, V. V. Bulatov, and S. Yip, "Molecular dynamics simulations of motion of edge and screw dislocations in a metal," *Computational materials science*, vol. 23, no. 1-4, pp. 111–115, 2002.

184. M.-C. Marinica, L. Ventelon, M. Gilbert, L. Proville, S. Dudarev, J. Marian, G. Bencteux, and F. Willaime, "Interatomic potentials for modeling radiation defects and dislocations in tungsten," *Journal of Physics: Condensed Matter*, vol. 25, no. 39, p. 395502, 2013.

185. P. Grigorev, A. M. Goryaeva, M.-C. Marinica, J. R. Kermode, and T. D. Swinburne, "Calculation of dislocation binding to helium-vacancy defects in tungsten using hybrid ab initio-machine learning methods," *Acta Materialia*, vol. 247, p. 118734, 2023.

186. A. H. Larsen, J. J. Mortensen, J. Blomqvist, I. E. Castelli, R. Christensen, M. Dułak, J. Friis, M. N. Groves, B. Hammer, C. Hargus, *et al.*, "The atomic simulation environment—a python library for working with atoms," *Journal of Physics: Condensed Matter*, vol. 29, no. 27, p. 273002, 2017.

187. P. Grigorev, T. D. Swinburne, and J. R. Kermode, "Hybrid quantum/classical study of hydrogen-decorated screw dislocations in tungsten: Ultrafast pipe diffusion, core reconstruction, and effects on glide mechanism," *Physical Review Materials*, vol. 4, no. 2, p. 023601, 2020.

188. E. Bitzek, P. Koskinen, F. Gähler, M. Moseler, and P. Gumbsch, "Structural relaxation made simple," *Physical review letters*, vol. 97, no. 17, p. 170201, 2006.

189. R. H. Doremus, "Diffusion in alumina," *Journal of Applied Physics*, vol. 100, p. 101301, 11 2006.

190. E. L. Kolsbjerg, M. N. Groves, and B. Hammer, "An automated nudged elastic band method," *The Journal of Chemical Physics*, vol. 145, p. 094107, 09 2016.

191. S. Makri, C. Ortner, and J. R. Kermode, "A preconditioning scheme for minimum energy path finding methods," *The Journal of Chemical Physics*, vol. 150, p. 094109, 03 2019.

192. S. J. Clark, M. D. Segall, C. J. Pickard, P. J. Hasnip, M. I. Probert, K. Refson, and M. C. Payne, "First principles methods using castep," *Zeitschrift für kristallographie-crystalline materials*, vol. 220, no. 5-6, pp. 567–570, 2005.

193. C. J. Pickard and R. Needs, "Ab initio random structure searching," *Journal of Physics: Condensed Matter*, vol. 23, no. 5, p. 053201, 2011.

194. N. Bernstein, G. Csányi, and V. L. Deringer, "De novo exploration and self-guided learning of potential-energy surfaces," *npj Computational Materials*, vol. 5, no. 1, p. 99, 2019.

195. E. V. Podryabinkin, E. V. Tikhonov, A. V. Shapeev, and A. R. Oganov, "Accelerating crystal structure prediction by machine-learning interatomic potentials with active learning," *Physical Review B*, vol. 99, no. 6, p. 064114, 2019.

196. C. J. Pickard, "Ephemeral data derived potentials for random structure search," *Physical Review B*, vol. 106, no. 1, p. 014102, 2022.

197. D. Vanderbilt, "Soft self-consistent pseudopotentials in a generalized eigenvalue formalism," *Physical review B*, vol. 41, no. 11, p. 7892, 1990.

198. M. Hart, J. Chen, A. Michaelides, A. Sella, M. S. Shaffer, and C. G. Salzmann, "One-dimensional arsenic allotropes: Polymerization of yellow arsenic inside single-wall carbon nanotubes," *Angewandte Chemie*, vol. 130, no. 36, pp. 11823–11827, 2018.

199. D. Schiferl and C. Barrett, "The crystal structure of arsenic at 4.2, 78 and 299 k," *Journal of Applied Crystallography*, vol. 2, no. 1, pp. 30–36, 1969.

200. P. Smith, A. Leadbetter, and A. Apling, "The structures of orthorhombic and vitreous arsenic," *Philosophical Magazine*, vol. 31, no. 1, pp. 57–64, 1975.

201. P. Silas, J. R. Yates, and P. D. Haynes, "Density-functional investigation of the rhombohedral to simple-cubic phase transition of arsenic," *Physical Review B*, vol. 78, no. 17, p. 174101, 2008.

202. L.-M. Liu, M. Krack, and A. Michaelides, "Density oscillations in a nanoscale water film on salt: Insight from ab initio molecular dynamics," *Journal of the American Chemical Society*, vol. 130, pp. 8572–8573, 11 2008.

203. Y. Chiang, "Muse: A python package for fast building amorphous solids and liquid mixtures," *github.com*, Dec. 2023. 10.5281/zenodo.10369245.

204. G. van Oudenaren, J. Ocadiz-Flores, and A. Smith, "Coupled structural-thermodynamic modeling of the molten salt system nacl-ucl3," *Journal of Molecular Liquids*, vol. 342, p. 117470, 2021.

205. D. Andersson and B. W. Beeler, "Ab initio molecular dynamics (aimd) simulations of nacl, ucl3 and nacl-ucl3 molten salts," *Journal of Nuclear Materials*, vol. 568, p. 153836, 2022.

206. L. P. N. Rebelo, V. Najdanovic-Visak, Z. P. Visak, d. P. M. Nunes, J. Szydlowski, C. A. Cerdeiriña, J. Troncoso, L. Romaní, J. M. S. S. Esperança, H. J. R. Guedes, and d. S. H. C., "A detailed thermodynamic analysis of [C4mim][BF4] + water as a case study to model ionic liquid aqueous solutions," *Green Chemistry*, vol. 6, no. 8, pp. 369–381, 2004.

207. E. Perlt, P. Ray, A. Hansen, F. Malberg, S. Grimme, and B. Kirchner, "Finding the best density functional approximation to describe interaction energies and structures of ionic liquids in molecular dynamics studies," *The Journal of Chemical Physics*, vol. 148, no. 19, p. 193835, 2018.

208. E. Gregoryanz, C. Ji, P. Dalladay-Simpson, B. Li, R. T. Howie, and H.-K. Mao, "Everything you always wanted to know about metallic hydrogen but were afraid to ask," *Matter and Radiation at Extremes*, vol. 5, no. 3, 2020.

209. I. B. Magdău, M. Marqués, B. Borgulya, and G. J. Ackland, "Simple thermodynamic model for the hydrogen phase diagram," *Physical Review B*, vol. 95, no. 9, p. 094107, 2017.

210. I. B. Magdău, F. Balm, and G. J. Ackland, "Theory of high pressure hydrogen, made simple," in *Journal of Physics: Conference Series*, vol. 950, 4, p. 042059, IOP Publishing, 2017.

211. C. J. Pickard, M. Martinez-Canales, and R. J. Needs, "Density functional theory study of phase iv of solid hydrogen," *Physical Review B*, vol. 85, no. 21, p. 214114, 2012.

212. I. B. Magdău and G. J. Ackland, "Identification of high-pressure phases iii and iv in hydrogen: Simulating raman spectra using molecular dynamics," *Physical Review B*, vol. 87, no. 17, p. 174110, 2013.

213. R. T. Howie, I. B. Magdău, A. F. Goncharov, G. J. Ackland, and E. Gregoryanz, "Phonon localization by mass disorder in dense hydrogen-deuterium binary alloy," *Physical review letters*, vol. 113, no. 17, p. 175501, 2014.

214. I. B. Magdău and G. J. Ackland, "Infrared peak splitting from phonon localization in solid hydrogen," *Physical review letters*, vol. 118, no. 14, p. 145701, 2017.

215. P. I. Cooke, I. B. Magdău, M. Peña-Alvarez, V. Afonina, P. Dalladay-Simpson, X.-D. Liu, R. T. Howie, E. Gregoryanz, and G. J. Ackland, "Raman signal from a hindered hydrogen rotor," *Physical Review B*, vol. 102, no. 6, p. 064102, 2020.

216. B. Cheng, G. Mazzola, C. J. Pickard, and M. Ceriotti, "Evidence for supercritical behaviour of high-pressure liquid hydrogen," *Nature*, vol. 585, no. 7824, pp. 217–220, 2020.

217. H. Zong, H. Wiebe, and G. J. Ackland, "Understanding high pressure molecular hydrogen with a hierarchical machine-learned potential," *Nature communications*, vol. 11, no. 1, p. 5014, 2020.

218. S. Frueh, R. Kellett, C. Mallery, T. Molter, W. S. Willis, C. King'ondu, and S. L. Suib, "Pyrolytic decomposition of ammonia borane to boron nitride," *Inorganic Chemistry*, vol. 50, pp. 783–792, 2 2011. doi: 10.1021/ic101020k.

219. A. Marfavi, P. Kavianpour, and L. M. Rendina, "Carboranes in drug discovery, chemical biology and molecular imaging," *Nature Reviews Chemistry*, vol. 6, pp. 486–504, 2022.

220. I. B. Sivaev and V. I. Bregadze, "Chemistry of nickel and iron bis(dicarbollides). a review," *Journal of Organometallic Chemistry*, vol. 614-615, pp. 27–36, 2000.

221. C. A. Brown and M. L. McKee, "Rearrangements in icosahedral boranes and carboranes revisited," *Journal of Molecular Modeling*, vol. 12, pp. 653–664, 2006.

222. F. Neese, "Software update: The orca program system—version 5.0," *WIREs Computational Molecular Science*, vol. 12, p. e1606, 9 2022.

223. A. S. Rosen, J. M. Notestein, and R. Q. Snurr, "Comprehensive phase diagrams of mos2 edge sites using dispersion-corrected dft free energy calculations," *The Journal of Physical Chemistry C*, vol. 122, no. 27, pp. 15318–15329, 2018.

224. D. Kieczka, T. Durrant, K. Milton, K. E. J. Goh, M. Bosman, and A. Shluger, "Defects in ws2 monolayer calculated with a nonlocal functional: any difference from gga?," *Electronic Structure*, vol. 5, no. 2, p. 024001, 2023.

225. Z. Fang, M. P. Confer, Y. Wang, Q. Wang, M. R. Kunz, E. J. Dufek, B. Liaw, T. M. Klein, D. A. Dixon, and R. Fushimi, "Formation of surface impurities on lithium–nickel–manganese–cobalt oxides in the presence of co2 and h2o," *Journal of the American Chemical Society*, vol. 143, no. 27, pp. 10261–10274, 2021.

226. E. Vanden-Eijnden and G. Ciccotti, "Second-order integrators for langevin equations with holonomic constraints," *Chemical Physics Letters*, vol. 429, no. 1, pp. 310–316, 2006.

227. H.-C. Wang, S. Botti, and M. A. Marques, "Predicting stable crystalline compounds using chemical similarity," *npj Computational Materials*, vol. 7, no. 1, p. 12, 2021.

228. H. Glawe, A. Sanna, E. K. U. Gross, and M. A. L. Marques, "The optimal one dimensional periodic table: A modified Pettifor chemical scale from data mining," *New Journal of Physics*, vol. 18, no. 9, p. 093011, 2016.

229. J. Riebesell, R. E. A. Goodall, Y. Chiang, A. Jain, P. Benner, K. A. Persson, and A. A. Lee, "Matbench Discovery – An evaluation framework for machine learning crystal stability prediction," *arXiv*, 2023.

230. D. Zagorac, H. Müller, S. Ruehl, J. Zagorac, and S. Rehme, "Recent developments in the Inorganic Crystal Structure Database: theoretical crystal structure data and related features," *J. Appl. Crystallography*, vol. 52, pp. 918–925, Oct 2019.

231. H. Pan, A. M. Ganose, M. Horton, M. Aykol, K. A. Persson, N. E. R. Zimmermann, and A. Jain, "Benchmarking coordination number prediction algorithms on inorganic crystal structures," *Inorganic Chem.*, vol. 60, no. 3, pp. 1590–1603, 2021.

232. S. Zhang, R. Schweitzer-Stenner, and B. Urbanc, "Do Molecular Dynamics Force Fields Capture Conformational Dynamics of Alanine in Water?," *Journal of Chemical Theory and Computation*, vol. 16, pp. 510–527, Jan. 2020.

233. B. Cantor, I. Chang, P. Knight, and A. Vincent, "Microstructural development in equiatomic multicomponent alloys," *Materials Science and Engineering: A*, vol. 375, pp. 213–218, 2004.

234. A. Mazitov, M. A. Springer, N. Lopanitsyna, G. Fraux, S. De, and M. Ceriotti, "Surface segregation in high-entropy alloys from alchemical machine learning," *arXiv preprint arXiv:2310.07604*, 2023.

235. A. P. Thompson, H. M. Aktulga, R. Berger, D. S. Bolintineanu, W. M. Brown, P. S. Crozier, P. J. in't Veld, A. Kohlmeyer, S. G. Moore, T. D. Nguyen, *et al.*, "Lammps-a flexible simulation tool for particle-based materials modeling at the atomic, meso, and continuum scales," *Computer Physics Communications*, vol. 271, p. 108171, 2022.

236. C. R. Trott, D. Lebrun-Grandié, D. Arndt, J. Ciesko, V. Dang, N. Ellingwood, R. Gayatri, E. Harvey, D. S. Hollman, D. Ibanez, N. Liber, J. Madsen, J. Miles, D. Poliakoff, A. Powell, S. Rajamanickam, M. Simberg, D. Sunderland, B. Turcksin, and J. Wilke, "Kokkos 3: Programming model extensions for the exascale era," *IEEE Transactions on Parallel and Distributed Systems*, vol. 33, no. 4, pp. 805–817, 2022.

237. A. Togo, "First-principles Phonon Calculations with Phonopy and Phono3py," *Journal of the Physical Society of Japan*, vol. 92, no. 1, p. 012001, 2023.

238. A. Togo, L. Chaput, T. Tadano, and I. Tanaka, "Implementation strategies in phonopy and phono3py," *Journal of Physics: Condensed Matter*, vol. 35, no. 35, p. 353001, 2023.

239. R. P. Stoffel, C. Wessel, M.-W. Lumey, and R. Dronskowski, "Ab Initio Thermochemistry of Solid-State Materials," *Angew. Chem. Int. Ed.*, vol. 49, no. 31, p. 5242, 2010.

240. C. J. Bartel, "Review of computational approaches to predict the thermodynamic stability of inorganic solids," *J Mater Sci*, Feb. 2022.

241. J. George, G. Hautier, A. P. Bartók, G. Csányi, and V. L. Deringer, "Combining phonon accuracy with high transferability in Gaussian approximation potential models," *J. Chem. Phys.*, vol. 153, p. 044104, July 2020. Publisher: American Institute of Physics.

242. "atomate2." https://github.com/materialsproject/atomate2.

243. A. Dunn, Q. Wang, A. Ganose, D. Dopp, and A. Jain, "Benchmarking materials property prediction methods: the Matbench test set and Automatminer reference algorithm," *Npj Comput. Mater.*, vol. 6, pp. 1–10, Sept. 2020. Number: 1 Publisher: Nature Publishing Group.

244. M. T. Agne, R. Hanus, and G. J. Snyder, "Minimum thermal conductivity in the context of *diffuson* -mediated thermal transport," *Energy Environ. Sci.*, vol. 11, no. 3, pp. 609–616, 2018.

245. W. Voigt, *Lehrbuch der kristallphysik: (mit ausschluss der kristalloptik)*. B.G. Teubner, 1910. Google-Books-ID: 9GISAAAAIAAJ.

246. A. Reuss, "Berechnung der fließgrenze von mischkristallen auf grund der plastizitätsbedingung für einkristalle .," *ZAMM - Journal of Applied Mathematics and Mechanics / Zeitschrift für Angewandte Mathematik und Mechanik*, vol. 9, no. 1, pp. 49–58, 1929. https://onlinelibrary.wiley.com/doi/pdf/10.1002/zamm.19290090104.

247. R. Hill, "The elastic behaviour of a crystalline aggregate," *Proc. Phys. Soc. A*, vol. 65, no. 5, p. 349, 1952.

248. J. Riebesell, E. Liu, J. Qi, T. W. Ko, and S. P. Ong, "MatCalc: A Python library for calculating materials properties," *github.com*, 2023. released July 2023, https://github.com/materialsvirtuallab/matcalc.

249. G. Kresse and J. Hafner, "Ab initio molecular-dynamics simulation of the liquid-metal-amorphous-semiconductor transition in germanium," *Phys. Rev. B*, vol. 49, p. 14251, 1994.

250. G. Kresse and J. Furthmüller, "Efficiency of ab-initio total energy calculations for metals and semiconductors using a plane-wave basis set," *Comput. Mat. Sci.*, vol. 6, p. 15, 1996.

251. P. J. Huber, "Robust estimation of a location parameter," in *Breakthroughs in statistics: Methodology and distribution*, pp. 492–518, Springer, 1992.

252. C. M. Bishop, *Neural networks for pattern recognition*. Oxford university press, 1995.

253. A. Wang, R. Kingsbury, M. McDermott, M. Horton, A. Jain, S. P. Ong, S. Dwaraknath, and K. A. Persson, "A framework for quantifying uncertainty in DFT energy corrections," *Scientific Reports*, vol. 11, p. 15496, July 2021.

254. R. S. Kingsbury, A. S. Rosen, A. S. Gupta, J. M. Munro, S. P. Ong, A. Jain, S. Dwaraknath, M. K. Horton, and K. A. Persson, "A flexible and scalable scheme for mixing computed formation energies from different levels of theory," *npj Computational Materials*, vol. 8, no. 1, p. 195, 2022.

255. J. Riebesell, "Pymatviz: visualization toolkit for materials informatics," *github.com*, 2022. 10.5281/zenodo.7486816 - https://github.com/janosh/pymatviz.

256. S. De, A. P. Bartók, G. Csányi, and M. Ceriotti, "Comparing molecules and solids across structural and alchemical space," *Physical Chemistry Chemical Physics*, vol. 18, no. 20, pp. 13754–13769, 2016.

257. G. Fraux, R. K. Cersonsky, and M. Ceriotti, "Chemiscope: Interactive structure-property explorer for materials and molecules," *Journal of Open Source Software*, vol. 5, no. 51, p. 2117, 2020.

258. L. McInnes, J. Healy, and J. Melville, "UMAP: Uniform Manifold Approximation and Projection for Dimension Reduction," 2020.